Journal of Computational Neuroscience 4, 103–127 (1997)

Oscillatory Mechanisms in Pairs of Neurons Connected with Fast Inhibitory Synapses

PETER F. ROWAT AND ALLEN I. SELVERSTON
Department of Biology, University of California at San Diego, La Jolla, CA 92093-0357
prowat@ucsd.edu
aselverston@ucsd.edu

Received July 24, 1995; Revised June 10, 1996; Accepted August 26, 1996

Action Editor: Eve Marder

Abstract. We study dynamical mechanisms underlying oscillatory behavior in reciprocal inhibitory pairs of neurons, using a two-dimensional cell model. We introduce one-and-two dimensional phase portraits to illustrate the behaviors, thus reducing the study of dynamical mechanisms to planar geometrical properties. We examined whether other mechanisms besides the escape and release mechanisms (Wang and Rinzel, 1992) might be needed for some cases of reciprocal inhibition, and show that, within the confines of a simple two-dimensional cell model, escape and release are sufficient for all cases. We divided the behaviors of a single cell into six different types and examined the joint behaviors arising from every combination of pairs of cells with behaviors drawn from these six types. For the case of two quiescent cells or two cells each having plateau potentials, bifurcation diagrams demonstrate the relations between synaptic threshold and synaptic strength necessary for oscillations by escape, oscillations by release, or network-generated plateau potentials. Thus we clarify the relationship between plateau potentials and oscillations in a cell. Using the two dimensional cell model we examine 1:N beating between cells and find that our simple model displays many of the essential dynamical properties displayed by more sophisticated models, some of which relate to thalamocortical spindling.

Keywords: CPG, escape and release mechanisms, frequency locking, motor pattern generation, nullcline, phase portrait, plateau potentials, synaptic threshold, two-dimensional cell model

1. Introduction

Our goal is to understand the principles underlying motor pattern generation by central pattern generators (CPGs). An isolated pair of connected neurons is the simplest example of a network that can generate a pattern, so is a good system with which to investigate basic questions about the functioning of small CPGs. Questions of interest include the following. Does the oscillatory behavior of a CPG arise from the oscillatory behavior of a single cell that then drives other cells to fire at different phases relative to this master cell, or does it arise as a network effect from the mutual interaction of several cells, none of which can individually oscillate, or does it arise from some combination of these two mechanisms? In the case of two nonoscillatory cells, is there just one or are there several mechanisms that may give rise to oscillations of the pair? The behavior generated by a CPG is defined primarily by the phase-relationships between bursts of the motor neurons contained in, or driven by, the CPG. A single CPG can give rise to several different behaviors when different neuromodulatory substances are applied (Selverston, 1993, Harris-Warrick and Marder, 1991). In the case of two connected cells, what physiological parameters influence most strongly the phase relationship between the two cells, and by what mechanism does this effect arise? Which parameters in a

pair of cells are most likely to be modified by neuromodulatory mechanisms? If there are several different possible mechanisms underlying oscillatory behavior in a pair of linked cells, can the mechanisms change as a result of neuromodulator application, and is there an experimental test to distinguish them?

One approach to the investigation of these questions is to use mathematical models. A useful model provides a formalization and summary of a wide range of data about a natural system, and may predict currently unknown regularities in their behavior. When the detailed workings of a model can be intuitively understood then the model may be used to make qualitative predictions without necessarily making extensive computations. If a mathematical model can be described with only a few equations, or equivalently is of low enough *dimension*, then its dynamics can be studied geometrically. This is done in the *phase portrait* of the model, which is a graphical representation of the model's dynamics. The phase portrait is constructed in the model's *phase space*, which has as many dimensions as there are differential equations in the model. When the model has only two differential, equations, then its phase space is two dimensional, and its dynamics can be studied in a planar phase portrait. Thus the study of cellular dynamics can, in the simplest case, reduce to geometric properties in the plane. Models with more than two equations have higher dimensional phase portraits, which are harder to visualize.

A pair of cells connected with reciprocal inhibition occurs in many small central pattern generators (Arbas and Calabrese, 1987; Arshavsky et al, 1993; Friesen & Stent, 1978; Getting, 1989; Kristan, 1980; Satterlie, 1985). Thus our initial goal is to understand the mechanisms underlying the oscillatory behavior of a reciprocal inhibitory pair of cells. Reciprocal inhibition between populations of neurons was proposed long ago by Brown (1914) as a pattern-generating mechanism for walking in cats. Perkel and Mulloney (1974) showed that alternate bursting could occur in two model neurons connected with reciprocal inhibition if each neuron had a slow intrinsic process giving rise to postinhibitory rebound. Satterlie (1985) found an example of two nonoscillatory cells, connected with reciprocal inhibition and each exhibiting postinhibitory rebound, that produced alternating bursts of spikes. Subsequently Wang and Rinzel (1992) showed that a reciprocal inhibitory pair of nonoscillatory model neurons, each having a current with fast activation and slow inactivation kinetics which gives rise to postinhibitory rebound (PIR) in the isolated cell, could generate an alternating rhythm. These authors found two distinct mechanisms, termed *release* or *escape*, that could underly the generation of alternating rhythms in this model. In the parameter range studied, either of these mechanisms could be responsible for oscillatory behavior. Skinner et al. (1994) extended Wang and Rinzel's results, showing that the release mechanism could be subdivided further into mechanisms called *intrinsic release* and *synaptic release*; the escape mechanism subdivides similarly. Experimentally, the difference between intrinsic and synaptic mechanisms is that for intrinsic mechanisms, overall oscillation frequency of the cell pair is insensitive to synaptic threshold, whereas when the oscillations occur by a synaptic mechanism, the pair frequency is sensitive to synaptic threshold.

Are there other mechanisms that may give rise to oscillatory behavior in a reciprocal inhibitory pair of cells, or are release and escape the only mechanisms available? We had previously noticed that there appeared to be several different mechanisms available for oscillations of an inhibitory pair of cells (Rowat and Selverston, 1993), especially since two nonoscillatory model cells, each having plateau potentials, could be made to oscillate when linked with reciprocal inhibition, but only in a small window of synaptic strengths. The original motivation for this study was to find all different dynamical mechanisms that could underly oscillations of a reciprocal inhibitory pair of neurons.

Due to the wide range of ionic channels known to occur in neural membranes (Hille, 1984, Llinas, 1988), one has to assume that many kinds of different neuronal dynamics may be possible. Thus we cannot *a priori* expect to list all possible different dynamical mechanisms underlying mutual oscillations in a pair of neurons. Our aim is, rather, to take two-dimensional cell model, that we hope is as simple as possible but not too simple, and use it to investigate and review the different dynamical mechanisms.

We use the cell model developed by (Rowat and Selverston, 1993) for a network model of the complete gastric mill CPG in the lobster, where it had the interesting property that when a network model was constructed with all the known connections between cells, the network model would automatically produce a rhythm roughly similar to the biologically observed rhythm with very little fine-tuning of parameters. Terman and Wang (1995) used a very similar cell model for a completely different purpose: as the nodes in a rectangular connected array of elements storing

a visual image. Using a locally excitatory, globally inhibitory architecture, the array correctly segments simple visual scenes. By analysis and simulation, it was shown that all oscillators representing a connected visual region synchronize rapidly, while blocks of oscillators corresponding to distinct connected regions become desynchronized.

Outline of the Paper. In the methods section we define the cell model and introduce phase portraits. We define six behavioral regimes of the model cell that correspond physiologically to endogenous oscillations, a quiescent cell, a state midway between the two previous regimes that we call "almost an oscillator," tonic depolarization (firing), chronic hyperpolarization; and plateau potentials. We show these states are characterized by geometric properties of the phase-portrait of the cell. These properties, in turn, correspond to specific relations amongst membrane currents.

In the results section we take pairs of cells with all possible different combinations of individual cell behaviors, connect them with fast-acting reciprocal inhibitory synapses, and investigate whether the resulting model inhibitory pair could, in some circumstances, oscillate. Since the model cells are two-dimensional and the synaptic transfer is immediate, the model of an inhibitory pair has a four-dimensional phase portrait, which is not easily visualized. As an alternative, we study a pair of linked two-dimensional single-cell phase portraits, where the phase portrait of each cell changes as a result of synaptic currents "generated" from the other phase portrait. We also investigate the generation of 1:N frequency-locked oscillations in a reciprocal inhibitory pair when one cell has the inward portion of its slow current smaller than the outward portion.

All the mechanisms in this paper use fast synapses: the postsynaptic current is an instantaneous function of the presynaptic membrane potential. This is a reasonable assumption if, as in the lobster gastric mill and pyloric CPGs,the oscillation period of the system under study is several orders of magnitude larger than the synaptic time course.

2. Methods

We introduce the cell model and also introduce one- and two-dimensional phase-portraits and their use in understanding the dynamics of a model. The phase-portrait is a well-known mathematical device for studying the dynamics of a system of equations (Wang and Rinzel, 1992; Somers and Kopell, 1993; Skinner et al., 1994). Our single cell phase-portrait is similar to the Fitzhugh (1961) single cell phase-portrait.

2.1. Definition of the Cell Model

Neurons have many different ionic membrane channels, but for the purpose of constructing a simple neural model we separate the corresponding membrane currents into two classes on the basis of their time constants: fast and slow. A single fast current is used to model the sum of all the fast currents, and a single slow current is used to model the sum of all the slow currents, both inward and outward. For example, the fast current could be the sum of a chloride leak current and a fast persistent sodium (Opdyke and Calabrese, 1994) or a fast persistent calcium current, while the outward part of the slow current could be the sum of potassium or calcium-gated potassium currents, and the inward part of the slow current could be carried by the same ions that contribute to I_h-type currents (Angstadt and Calabrese, 1989; Golowasch and Marder, 1992; McCormick and Pape, 1990). The fast current is assumed to activate immediately. The slow current's time constant for activation, τ_s, is assumed to be significantly slower than the membrane time constant τ_m. We have usually taken the ratio of τ_s to τ_m to be about 20, but even when the ratio is as small as 1.5, most model phenomena dependent on the difference in time constants still arise. Spikes are not included in the model because for some CPGs, in particular for the ones of most direct interest to us, the gastric mill and pyloric CPGs in the lobster, pattern generation is little affected when spikes are suppressed (Anderson and Barker, 1981; Raper, 1979a). Therefore we ignore spike-based synaptic transmission and model the communication between cells by graded synaptic transmission alone.

The model cell has two differential equations, one for the membrane potential V, derived from current conservation, and one for the lumped slow current q, derived from current activation:

$$\tau_m \frac{dV}{dt} = -(\text{fast}(V, \sigma_f) + q - i_{\text{inj}}) \tag{1}$$

$$\tau_s \frac{dq}{dt} = -q + q_\infty(V) \tag{2}$$

$$\tau_m < \tau_s. \tag{3}$$

V and q describe the state of the model so are called *state variables*. Due to the difference in time constants (3), Eq. (1) is called the *fast equation*, and Eq. (2) the *slow equation*. The other quantities are τ_m = membrane time constant; i_{inj} = injected current; i = fast(V, σ_f) is an idealized current-voltage (IV) curve for the lumped fast current where

$$\text{fast}(V, \sigma_f) = V - A_f \tanh((\sigma_f / A_f)\, V). \qquad (4)$$

This expression for the fast IV curve has the following property: the slope of the "reverse" part of the N is given by $\sigma_f - 1$, and the width of the N is given by A_f. Thus the degree of N-shape in the fast IV curve is controlled by the parameter σ_f as follows (Fig. 1(a)): the IV curve is N-shaped when $\sigma_f > 1$, and the degree of N-shape increases with increasing σ_f; it has an inflexion point when $\sigma_f = 1$; and it is linear when $\sigma_f = 0$. τ_s is the activation time constant for the lumped slow current q. The steady-state value of the lumped slow current is linear in V, with conductance σ_s for both the inward and outward parts, and having reversal potential E_s (Fig. 1(b)):

$$q_\infty(V) = \sigma_s (V - E_s). \qquad (5)$$

In a small extension to the model, the slow current is split into two linear parts, an inward part with conductance σ_{in} and an outward part with conductance σ_{out} (Fig. 1(c)), where $\sigma_{\text{in}} < \sigma_{\text{out}}$ to incorporate the fact that inward slow currents generally have a smaller conductance than outward slow currents. In this case the following expression is used for the lumped slow current:

$$q_\infty(V) = \begin{cases} \sigma_{\text{in}}(V - E_s) & \text{if} \quad V < E_s \\ \sigma_{\text{out}}(V - E_s) & \text{if} \quad V > E_s. \end{cases} \qquad (6)$$

The left column of Fig. 1 shows the IV curves for the fast and slow currents: i = fast(V, σ_f) in 1a and $i = q_\infty(V)$ in 1b and c.

Note that the variable q represents a *current* and not the activation of a conductance. q approaches the steady-state value $q_\infty(V) = \sigma_s(V - E_s)$ with time constant τ_s. Equation (2) with (5) is unusual because the reversal potential for the lumped slow current, E_s, appears here and not in the current Eq. (1). Thus this model might be called semi-conductance-based.

The fast current can be considered to be the sum of a leak current and an inward Ca^{++} current, with $\sigma_f = g_{\text{Ca}}/g_L$, and the slow current q can be considered to be a slow potassium current with $\sigma_s = g_K/g_L$.

Dimensions. As can be seen from Eq. (1), q and i_{inj} both have the dimension of an electrical potential. A true current is obtained by multiplying the model current by a leak conductance g_L. That is, a current is represented by the potential sufficient to drive the current through the membrane leak conductance (a constant). If, for example, q is taken to represent a slow potassium current, the actual current flowing is obtained by multiplying q by g_L. Similarly the true injected current corresponding to i_{inj} is obtained by multiplying by g_L. Thus, τ_m and τ_s are in msec., V, E_s, q, and i_{inj} are in mV, σ_f is a dimensionless shape parameter, and σ_s is dimensionless since it is a conductance normalized to the leak conductance.

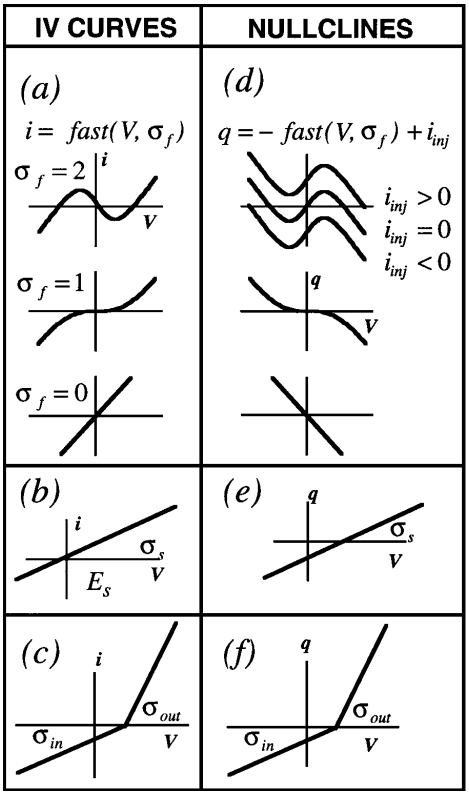

Figure 1. IV curves and nullclines in the cell model. (a) The curve $i = \text{fast}(V, \sigma_f)$ for three values of σ_f. (b) The standard slow current IV curve. E_S is the reversal potential. (c) The split slow current IV curve with different inward and outward conductances. (d) The V-nullcline for $\sigma_f = 2, 1, 0$. For $\sigma_f = 2$, three values of the injected current produce three positions of the V-nullcline. (e) The q-nullcline. (f) The q-nullcline when using a split slow current. A fast current null cline is obtained by reflecting the IV curve of the fast current in the V-axis and then moving it up or down by the amount of the injected current. A slow current nullcline is identical with the IV curve of the slow current.

One-Dimensional Phase Portraits. The equation

$$\tau_m \frac{dV}{dt} = -(V + q),$$

where q is held fixed at $q = q_0$, has a single state variable V and has a single fixed point at $V = -q_0$ when $\frac{dV}{dt} = 0$. The system has a one-dimensional phase portrait, shown in Fig. 2(a).

The line portrays the range of values of V, the black dot is the fixed point at $V = -q_0$, and the arrows show that whatever the value of V when the system is started, it moves to the fixed point. In one dimension, fixed points are either *stable* or *unstable*; experimentally, only stable fixed points fixed points are seen. In the example here, the fixed point is stable because if V is displaced slightly—say, to $V = -q_0 + \delta$ where δ is small—V returns to $V = -q_0$ with time constant τ_m. Figure (2b) shows a stack of one-dimensional phase portraits for three values of q, with vertical spacing proportional to q. Note that the fixed points lie on the line $q = -V$.

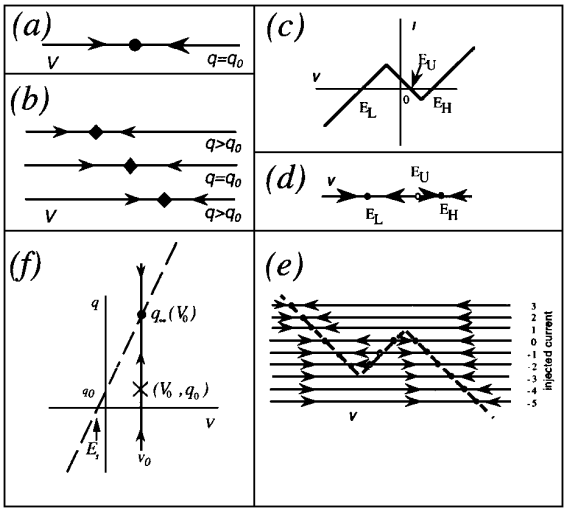

Figure 2. One-dimensional phase portraits. (a) A one-dimensional phase portrait with a single stable fixed point. (b) Stack of three one-dimensional phase portraits. (c) The piecewise linear IV curve used for $i = \text{fast}(V, 2)$ in Eq. (15) (d)The one-dimensional phase portrait of Eq. (7) with $q = 0$. Solid circles are stable fixed points (attractors), hollow circle is an unstable fixed point (repellor). (e) Stack of one-dimensional phase portraits for nine values of q in Eq. (7). The dashed line connecting the fixed points of the one-dimensional phase portraits is the curve of part (*c*) reflected in the V-axis, $q = -\text{fast}(V, 2)$. (f) The thick vertical line is the one dimensional phase-portrait for equation(8), when V is fixed at $V = V_0$. The dashed line is the line $q = q_\infty(V)$.

More generally, consider the equation

$$\tau_m \frac{\mathrm{d}V}{\mathrm{d}t} = -\big(\text{fast}(V, \sigma_f) + q\big), \tag{7}$$

where q is held fixed at $q = q_0$. Take $\sigma_f > 1$ so the IV curve $i = \text{fast}(V, \sigma_f)$ has a region of negative resistance. For illustrative purposes we use a schematic, piecewise linear, form for the IV curve of the fast current, shown in Fig. 2(c).

The fixed points of Eq. (7) are values of V for which $q_0 = -\text{fast}(V, \sigma_f)$. When $\sigma_f = 2$ and $q_0 = 0$ there are three fixed points, labelled E_L, E_U, E_H in Fig. 2(c). The curve $q_0 = -\text{fast}(V, 2)$ is the reflection of the curve of Fig. 2(c) in the V-axis. Thus the associated one–dimensional phase portrait has three fixed points labelled E_L, E_U, and E_H, as shown in Fig. 2(d). E_L and E_H are stable fixed points, while E_U is unstable.

In Fig. 2(e) we have kept $\sigma_f = 2$ in (7) and aligned the one-dimensional phase portraits for several different values of q in a vertical stack. As q is increased from $q = -5$, the one–dimensional phase portrait changes from having a single stable fixed point on the right leg of the N-shaped curve, to having three fixed points (the center one unstable), to having single fixed point on the left leg. A "jump" was forced to occur where the number of fixed points changed from three to one at the tip of the upward-pointing knee. Similarly if q is reduced from $q = 3$, a rightward jump will be forced between $q = -2$ and $q = -3$. Clearly if there was a means of increasing q slowly when V is to the right of the peak in $-\text{fast}(V, \sigma_f)$, and decreasing q slowly when V is to the left of the dip in $-\text{fast}(V, \sigma_f)$, oscillations would occur. Such a mechanism is provided by the following Eq. (8), which also has a one-dimensional phase portrait.

Consider the equation

$$\tau_s \frac{\mathrm{d}q}{\mathrm{d}t} = -q + q_\infty(V), \tag{8}$$

where $q_\infty(V) = \sigma_s(V - E_s)$. If V is held fixed at $V = V_0$—for example, by voltage clamp—and initialize $q = q_0$, then q will rise or fall to its steady-state value $q_\infty(V_0)$. This is shown in Fig. 2(f) as a vertical, one-dimensional phase-portrait with a single fixed point. If we appropriately combine the vertical phase portrait of Fig. 2(f) with the horizontal phase portraits of Fig. 2(e), oscillations will occur.

The key is the location of the line $q = q_\infty(V)$ relative to the curve $q = -\text{fast}(V, \sigma_f)$. The right leg of the dashed line in Fig. 2(e) should be below the dashed

line in Fig. 2(f), thus causing q to increase slowly, and the lefthand leg of the dashed line in Fig. 2(e) should be above the dashed line of Fig. 2(f), thus causing q to decrease slowly. This occurs if the two dashed lines intersect between the peak and dip in Fig. 2(e).

Note also that the speeds of movement in these one-dimensional horizontal and vertical phase-portraits have simple relationships to the geometry of Fig. 2(e) and 2(f). The horizontal speed of movement on one of the one-dimensional phase-portraits in Fig. 2(e) is, by Eq. (7),

$$-\frac{1}{\tau_m}(q_0 - (-\text{fast}(V, \sigma_f)). \tag{9}$$

This is proportional to the vertical distance from the point V of the one-dimensional phase-portrait at q_0 to the short-dashed curve. Similarly, the vertical speed of movement on the one-dimensional phase-portrait at $V = V_0$ in Fig. 2(f) is, by Eq. (8),

$$\frac{1}{\tau_s}(q_\infty(V_0) - q), \tag{10}$$

which is proportional to the vertical distance from the point $q_\infty(V_0)$ on the line of large dashes to the current state q.

Two-Dimensional Phase Portraits. The Eqs. (7) and (8) constitute the model cell. This is a two-dimensional system of differential equations with state variables V and q. As the state evolves in time it describes a curve in the (V, q) phase-plane called a *trajectory*. Figures 3(b) and 3(c) show a two-dimensional phase portrait and the corresponding potential trace for an endogenously oscillating cell model. The dots in Fig. 3(b) are consecutive states of the system at equal time intervals. At each point there are horizontal and vertical components to the movement, which can be approximately represented by one-dimensional phase portraits as described in the previous section. See also Figs. 3(a1), (a2), (a3). Every state variable in a model has a *nullcline*, defined to be the line of points in phase space at which the time-derivative of the state variable is zero. In dimension 3, a nullcline is a surface, and in general, in dimension n a nullcline has dimension $n-1$. They are very useful in understanding the motion of the state of the system in phase space. For example, the time derivative of a state variable has opposite sign on opposite sides of that variable's nullcline. In the model cell, the phase space is a plane and the V-nullcline is the

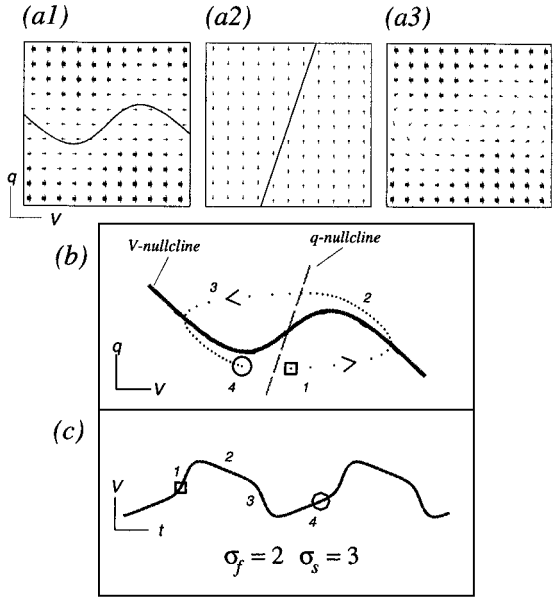

Figure 3. The relation between one- and two- dimensional phase-portraits and the phase portrait for the endogenously oscillating cell model. In (a1), (a2), and (a3), the strength of the "vector field" at each point is denoted by the thickness and direction of the arrows. In (a1), the horizontal component ($\frac{dV}{dt}$) generated by Eq. (7) is plotted, together with the V-nullcline. Note that the direction of the arrows changes when the V-nullcline is crossed. In (a2), the vertical components ($\frac{dq}{dt}$) generated by Eq. (8) have been plotted. Again, note the change in direction when the q-nullcline is crossed. The field is too weak for the variation in strength with position to be visible. The combined field ($\frac{dV}{dt}$, $\frac{dq}{dt}$) is plotted in (a3). (b) The (V, q) phase plane for the cell model, including the V and q-nullclines and a trajectory (dotted curve). The state of the cell (V, q), as it evolves by Eqs. (7) and (8), follows this trajectory when transients have died out. The dots are drawn at equal time intervals, hence the spacing signifies speed. The movements on the right and left legs of the N-shaped fast nullcline are slow compared to the rapid, roughly horizontal, movements on the upper and lower segments. Thus one cycle consists of two slow segments separated by two horizontal jumps. The notations 1, 2, 3, and 4 identify corresponding points on the trajectory in the (V, q) phase-plane and membrane potential trace in (c). The trajectory is snake-like, with the snake's head marked by a circle and its tail by a square; corresponding positions on the traces are marked. (c) Voltage trace corresponding to the trajectory in (b). In this and other figures, unless specified otherwise, $\tau_m/\tau_s = 1/20$.

curve defined by $\frac{dV}{dt} = 0$ — namely,

$$q = -\text{fast}(V, \sigma_f) + i_{\text{inj}}. \tag{11}$$

This divides the phase plane into two regions, one where the V-component of motion on a trajectory is leftward and one where the V-motion is rightward (Fig. 3(a1)). Similarly, the q-nullcline, defined by $\frac{dq}{dt} = 0$, divides the plane into two regions with the q-components of motion in opposite directions

(Fig. 3(a2)). Any trajectory crosses the V-nullcline vertically, since $\frac{dV}{dt} = 0$, and the q-nullcline horizontally, since $\frac{dq}{dsFig.t} = 0$. Points of intersection of the nullclines are fixed points. These facts often enable one to deduce useful properties of a model without solving the model equations.

Physiologically, the V-nullcline can be described in terms of a membrane potential recording as follows. The V-nullcline consists of exactly those points in phase-space at which turning points—maxima and minima—of the trace can occur. At a turning point the trace is momentarily horizontal, so the fast and slow currents must be exactly in balance. Therefore the slow current is exactly equal and opposite to the fast current, so the V-nullcline is obtained by reflecting the IV-curve of the fast current in the V-axis. A depolarizing (hyperpolarizing) injected current moves the fast IV curve downward (upward), so the V-nullcline is moved upward (downward). Physiologically, the q-nullcline is the same as the IV curve for the lumped slow currents.

Figure 1(d) shows examples of the fast nullcline for $\sigma_f = 0$, 1, and 2, and, for $\sigma_f = 2$, it shows how an injected current shifts the fast nullcline up or down. Figure 1(e) and (f), show that the q-nullcline $q = q_\infty(V)$ is identical with the steady-state IV curve $i = q_\infty(V)$.

At each point in the phase plane, the movement has a horizontal component given by Eq. (9) and a vertical component given by Eq. (10). By Eq. (3), $1/\tau_m$ is much larger than $1/\tau_s$. Hence, at a general position in the phase plane away from the fast nullcline, the horizontal component of velocity is much larger than the vertical component. So in predicting the movement of the state in this two-dimensional phase portrait, the vertical or q-component can be regarded as approximately constant until the rapid horizontal movement of V brings the state (V, q) close to the fast nullcline. Then the slow equation begins to take effect while the fast Equation now serves merely to hold the state close to the fast nullclline. Thus the motion on segments 1 and 3 of the trajectory in Fig. 3(b), away from the fast nullcline, is essentially controlled by Eq. (7) as depicted by the one dimensional phase portraits in Fig. 2(e). The vertical motion when close to the fast nullcline is controlled by one-dimensional phase portraits as in Fig. 2(f). This reduction of the movements in phase-space into fast horizontal jumps between slow movements along the fast nullcline, valid when there is a large difference between time constants as in (3), is known mathematically as a *singular decomposition*, or the *relaxation regime*.

The fastest horizontal movements in the phaseplane—points of steepest ascent or descent on the traces—occur where the vertical distance from trajectory to V-nullcline is greatest, by Eq. (9). This can be confirmed in Fig. 3(b) where the greatest spacing between dots occurs beneath the peak and above the dip in the V-nullcline. The speed of vertical movement in the phaseplane, which corresponds to the angle of descent on segment 2 of the trajectory or of ascent on segment 4 (Fig. 3(c)), is proportional to the vertical distance from trajectory to q-nullcline (by (10)).

2.2. *Properties of the Cell Model*

Frequency Control. In this cell model the majority of the time in each cycle is spent on the slow segments, where the speed is proportional to the vertical distance to the q-nullcline. Since this depends on the slow conductance σ_s, σ_s is the primary determinant of cycle frequency. This is not a parameter easily manipulated experimentally. In most neurons, the oscillation frequency varies with injected current, a phenomenon not well captured by our model. Typically in a conductance-based model (for a particularly simple example see Morris and Lecar, 1981), injected current shifts the fast nullcline and changes the size of its N-shaped part; since this alters the distances traveled under control of the slow equation, the cycle frequency changes. This lack in our model is made up to some extent by its simplicity, while still able to capture many aspects of network interactions.

A simple alternative way to obtain an increase of frequency with injected current is to utilize the "narrow channel" effect: if two nullclines in the phase plane come close together in a certain region without crossing, then, in this region, the phase point must necessarily move very slowly, since it is close to two lines on each of which one component of the phase point velocity is zero. This effect was used by Hindmarsh and Rose (1984) and Rose and Hindmarsh (1985) in developing three-dimensional neural models. For example, suppose we deform the slow nullcline by curving its inward current portion round so that it passes close to the downward pointing knee of the fast nullcline. Physiologically, an A-current might cause this deformation. This is not the same as the split slow current extension, Eq. (6). The effect is to greatly slow down the approach of the phase point to the knee, so the interburst interval on the voltage trace is much larger than each burst. Any depolarizing injected current increases the distance from the knee to the slow nullcline, thus reducing the narrow channel effect, with a resulting increase of frequency. An example is shown in Fig. 4. Comparable effects are seen in a small CPG in *Clione* (Arshavsky et al., 1991).

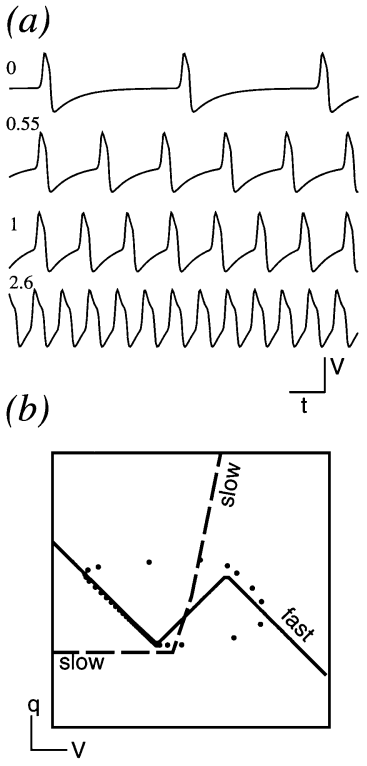

Figure 4. Control of frequency by current when the slow nullcline has a flat inward portion. (a) Increase in frequency with depolarizing injected current. The figure by each trace is the injected current. (b) The phase portrait showing inward current saturation level of the q-current IV-curve. Parameter values: $\sigma_f = 2$, $A_f = 1$, $\sigma_s = 8$, q-current inward portion becomes constant at -0.55, $\tau_m = 0.05$, $\tau_s = 1.8$.

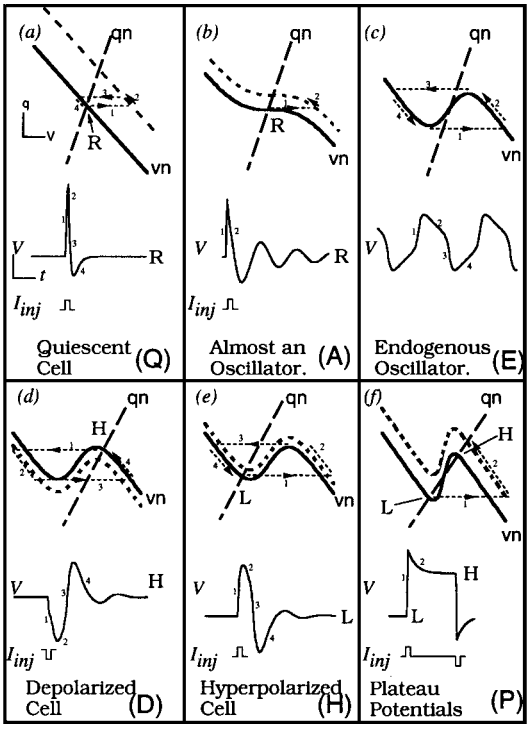

Figure 5. The six intrinsic of behaviors of the cell model: Q, A, E, D, H, P. Each box shows the phase portrait on the $(V, q)-$phase plane, corresponding membrane potential trace, and I_{inj} trace. The V- and q- nullclines are labeled with vn (solid line) and qn (long dashes). During a current pulse the V-nullcline is shifted to a new position, shown by a thick dotted line in all cases except (c) where no pulse occurs. The trajectories are sketched with thin dashed lines and arrows. Numerical notations show correspondences between trajectories and traces. Times of depolarizing and hyperpolarizing current pulses are shown on the I_{inj} trace. $\sigma_f = 0$ in (a), 1 in (b), 2 in (c), (d), and (e), and 4 in (f).

Intrinsic Behaviors. Six intrinsic behaviors of the model cell, obtained with different settings of the cellular parameters, correspond to six physiological behaviors: stable resting potential or quiescence (Q), almost an oscillator (A), endogenous oscillations (E), permanent depolarization (D) with tonic firing in a spiking cell, permanent hyperpolarization (H), and plateau potentials (P). These behaviors are shown in Fig. 5.

Endogenous oscillations (Fig. 5(c)) occur when the V-nullcline has a region of negative resistance ($\sigma_f > 1$), and the slow and fast nullclines intersect between the peak and dip in the V-nullcline. The single fixed point is always unstable. The model is "almost an oscillator" (Fig. 5(b)) when the V-nullcline has a point of inflexion ($0 < \sigma_f \leq 1$). During a depolarizing pulse the state moves rapidly rightwards toward the V-nullcline at its new position (thick dashed curve), and when the pulse terminates the trajectory spirals into the fixed point, giving a damped oscillatory trace. The cell is quiescent (Fig. 5(a)) when the V-nullcline is linear ($\sigma_f = 0$). As in Fig. 5(b) a current pulse causes the state to jump right to the new temporary V-nullcline and then to move up the V-nullcline toward the new fixed point. When the pulse ends the state jumps back left on to the original V-nullcline at a value of V below the resting potential, then slowly returns to the rest potential R. The cell has plateau potentials (Fig. 5(f)) when the q-nullcline intersects the N-shaped V-nullcline ($\sigma_f > 1$) in three fixed points. The low(L) and high (H) ones are stable, giving rise to plateau potentials; the center fixed point is unstable (not labeled). In the trace, the cell is started at the low potential then a depolarizing pulse causes the state to jump toward the right leg of the V-nullcline, which is in a new position for the duration of the pulse. On pulse termination the state relaxes toward the high fixed point (H). The exact trajectory taken depends critically on the duration of the pulse. At a minimum, the

pulse must be long enough for the state to cross the V-nullcline in its original position between the dip and peak, before the pulse terminates. A hyperpolarizing pulse applied to the cell at H switches the cell back to L. The cell is permanently hyperpolarized (Fig. 5(e)) when the q-nullcline intersects the V-nullcline exactly once, at a fixed point L to the left of the downward knee in the V-nullcline. A depolarizing pulse in the correct amplitude range results in one loop in phase space returning to rest at L. The pulse amplitude must be large enough to raise the q-coordinate of the downward knee in the V-nullcline above the q-coordinate of L and long enough for the state to cross the original position of the V-nullcline once. If L is close to the downward knee a small damped oscillation occurs after the main loop. A hyperpolarizing pulse has little effect. The cell is permanently depolarized (Fig. 5(d)) when a single intersection point occurs at H to the right of the upward knee in the V-nullcline. Similarly to Fig. 5(e), a depolarized pulse causes a single excursion and return to H.

When the fast nullcline is N-shaped the cell is either an endogenous oscillator (Fig. 5(c)), has plateau potentials (Fig. 5(f)), is permanently hyperpolarized (Fig. 5(e)), or is permanently depolarized (Fig. 5(d)). In the latter case, if spike generation were included in the model, the cell would be firing tonically. Which behavior occurs depends on the number and location of the points of intersection of the slow nullcline with the fast nullcline. Three points of intersection causes plateau potentials, as shown in Fig. 5(f). A single intersection point, on the left leg of the fast nullcline, causes a hyperpolarized rest potential as in Fig. 5(e); one on the center leg causes oscillations since it is unstable (Fig. 5(c)); while one on the right leg causes a depolarized rest potential (Fig. 5(d)). If the fast nullcline is not too N-shaped then the cell has a rest potential R and after a current pulse it may exhibit damped oscillations (5b) or return immediately to rest (5a). When oscillating, most of the cycle time is occupied by the slow movements up and down the right and left legs of the fast nullcline; these correspond to the burst and interburst intervals. As we have seen, this primarily depends on the slow conductance parameter σ_s (or σ_{in} and σ_{out}); hence the cycle time, or frequency, is determined primarily by these parameters. If σ_{in} is less than (greater than) σ_{out}, then the interburst interval will be longer (shorter) than the burst duration.

The only difference between panels (c), (d), and (e) is the relative position of the fast and slow nullclines. This can be manipulated by the amount and sign of the injected current (cf. Fig. 1(d)). Thus a model cell originally firing tonically (behavior D, Fig. 5(d)), will change to endogenous oscillations (behavior E, 5(c)) and then to permanent hyperpolarization (behavior H, Fig. 5(e)) as hyperpolarizing current is injected. Similarly, depolarizing current could cause a transition from case H to E to D. In the terminology of (Elson and Selverston, 1992), a cell with this behavior is said to have *bursting pacemaker potentials*.

If model cell has a split slow current (Fig. 1(c)), then the *duty cycle*, defined to be the ratio of the burst interval to the time for one complete cycle, will be less than (greater than) 0.5 if $\sigma_{\text{in}} < \sigma_{\text{out}}$ ($\sigma_{\text{in}} > \sigma_{\text{out}}$).

Bifurcation Diagrams. The relationship between the behaviors of a model as parameters vary is conveniently summarized in a *bifurcation diagram*. In the model cell, if the time constants and the size of the N, A_f, are kept fixed, there are three parameters, σ_f, i_{inj}, and σ_s, that define a three-dimensional space. Then one plots the behavior associated with each point of this space. In Fig. 6, we set $\sigma_s = 2$ and plotted the behaviors in the $(\sigma_f, i_{\text{inj}})$ plane. The vertical dotted line shows the behavior transitions H-E-D that could occur in response

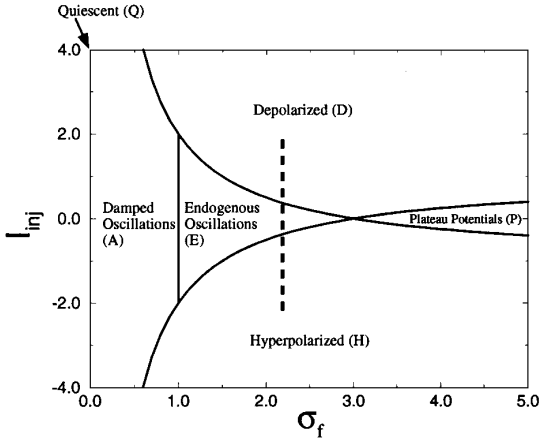

Figure 6. Bifurcation diagram for the model cell. The $\sigma_f - I_{\text{inj}}$ plane is divided into regions corresponding to different cell behaviors for fixed $\sigma_s = 2$. The quiescent cell (Q) region is the I_{inj} axis. A = almost an oscillator, E = endogenous oscillations, D = depolarized cell (tonic firing if spikes present), H = hyperpolarized cell, P = plateau potentials. Vertical dashed line shows effects of different amounts of injected current.

The bifurcation diagrams (Figs. 6, 10, and 12) are not claimed to be exact or even complete. They were drawn using the geometry of the phase portraits, assuming that the singular decomposition was in effect, so all jump motions are assumed to be horizontal and the time required for the "escape" or "release" switches to occur have been ignored. When these times are taken into account one finds that oscillations cannot occur when the putative trajectory would spend too little time across threshold (for example, when the threshold in release is toward the high end of the range). Thus the regions of oscillation in the figures are, in general, slightly too large.

to varying the injected current. The figure shows that the transition H to P (plateau potentials) to D is another possible response to increasing injection of depolarizing current. A central horizontal line followed from left to right goes through behavior regions Q, A, E, P, corresponding to panels a, b, c, and f in Fig. 5. A more depolarized (or hyperpolarized) line passes through behavior regions Q-A-E-D-P or Q-A-E-H-P).

2.3. *Model of a Pair of Cells with Reciprocal Inhibition*

Each synapse onto a cell is modeled by adding a synaptic current into the fast Eq. (1) or (7) as follows:

$$\tau_m \frac{dV}{dt} = -(\text{fast}(V, \sigma_f) + q + i_{\text{syn}} - i_{\text{inj}}) \qquad (12)$$

where

$$i_{\text{syn}} = W\ f(V_{\text{pre}})(V - E_{\text{post}}). \qquad (13)$$

W is the maximum postsynaptic conductance, V_{pre} is the pre-synaptic potential, E_{post} is the synaptic reversal potential, and

$$f(V) = \left(1 + e^{-\gamma(V-\theta)}\right)^{-1} \qquad (14)$$

is a sigmoid *synaptic transfer* function with threshold θ and gain γ. Each synapse contributes another postsynaptic current i_{syn} to Eq. (11). Here θ is the threshold for graded synaptic transmission, which in general is different from the threshold for action potentials; the latter does not enter into this model. A synapse is excitatory if i_{syn} is depolarizing that is, if E_{post} is higher than the maximum post-synaptic membrane potential during oscillatory behavior; it is inhibitory if the postsynaptic current is hyperpolarizing, by having E_{post} below the minimum of the postsynaptic membrane potential.

A network of two reciprocal inhibitory cells, which we call an inhibitory pair (IP), has a model with four equations. Each cell has Eq. (12) for its fast equation, using expression (13) for the synaptic current, and Eq. (8) for its slow equation. Thus the IP model has a four-dimensional phase space and a four-dimensional phase portrait. We study this as two linked two-dimensional phase portraits, one for each cell. In the two-dimensional phase portrait of each cell, the position and shape of the fast nullcline varies with the synaptic current being received.

At this point we simplify the model further. We replace each sigmoid synaptic transfer function by a 0-1 step function with threshold θ, equivalently by letting the gain $\gamma \to \infty$ in (14). Thus the postsynaptic conductance is either fully on or off, depending on whether the presynaptic cell's membrane potential is above or below the threshold θ. Hence the fast nullcline in the postsynaptic cell has exactly two distinct positions, depending on whether i_{syn} is on or off. We also replace, in each cell, the curvilinear form of the fast IV curve (Eq. (4)) by piecewise linear approximation, defined by

$$\text{fast}(V, \sigma_f) = \begin{cases} V + A_f & \text{for } V < -A_f/\sigma_f \\ V - A_f & \text{for } V > A_f/\sigma_f \\ (1 - \sigma_f)V & \text{otherwise.} \end{cases} \qquad (15)$$

3. Results

We systematically investigated the oscillatory capability of each combination of pairs of the intrinsic cellular behaviors (Q, A, E, D, H, P) in a reciprocal inhibitory pair. There are 21 different combinations, and we report in detail only on cases QQ, QD, and PP. Figure 7

Figure 7. There are 21 different reciprocal inhibitory pairs of cells, when each cell has one of the six intrinsic behaviors of Fig. 5. In each case the weights and thresholds have been adjusted to produce oscillatory behavior. For each case we show the two membrane potential traces (upper part) and the corresponding phase portraits for each cell (lower part).

E = endogenous oscillator, A = almost an oscillator, Q = quiescent cell, D = depolarized, H = hyperpolarized, P = Plateau potentials. The top trace in each pair is generated by the cell with the left phase-portrait.

Parameters are given in the order $(W_{12}, W_{21}, \theta_{21}, \theta_{12}, \sigma_{f1}, \sigma_{f2}, \sigma_{s1}, \sigma_{s2})$. In all cases in this and subsequent figures, $E_{\text{post}} = -4$, $\gamma = 40$, and $\tau_m/\tau_s = 1/20$. Injected current, if present, is listed separately. QQ = (0.4, 0.4, 0.2, 0.2, 0, 0, 3, 3), QA = (0.1, 0.3, 0, 0, 1, 0, 3, 3), QE = (0.1, 0.4, 0.7066, 0.73333, 2, 0, 3, 3), QD = (0.1, 0.1, 0.1, 0.58666, 0, 3, 3, 3), $i_2 = 0.76$, QH = (0.3, 0.3, −0.6, −0.8, 0, 4, 2, 4), $i_1 = -0.4$, $i_2 = -0.50666$, QP = (0.3, 0.3, 0.10666, 0.4, 0, 4, 2, 2.3), AA = (0.2, 0.2, 0, −0.01333, 1, 1, 2, 2), $i_1 = i_2 = 0.4$, AE = (0.1, 0.1, 0.1, 0.1, 2, 1, 3, 3), AD = (0.1, 0.1, −0.586667, 0.09333, 4, 1, 3, 2), AH = (0.1, 0.1, 0.81333, 0.09333, 4, 1, 3, 2), $i_1 = -0.36$, AP = (0.1, 0.34, 0, 0.62666, 1, 4, 3, 3), EE = (0.1, 0.1, 0.1, 0.1, 2, 2, 3, 3), ED = (0.1, 0.3, 0.16, 0.73333, 2, 4, 3, 3), $i_2 = 0.7$, EH = (0.1, 0.3, 0.16, 0.73333, 2, 4, 3, 3), $i_2 = 0.7$, EP = (0.1, 0.1, 0.7066, 0.73333, 2, 4, 3, 2), DD = (0.3, 0.3, 0.50666, 0.50666, 4, 4, 2, 2), $i_1 = i_2 = 0.4$, DH = (0.1, 0.1, −0.61333, 0.77333, 3, 3, 3, 3), $i_1 = -i_2 = 0.56$, DP = (0.22, 0, −0.85333, −0.54667, 3, 3, 1.4, 1.8), $i_1 = 0.04$, $i_2 = 0.6133$, HH = (0.2, 20.2, −1, −1, 4, 4, 3, 3), $i_1 = i_2 = -0.24$, HP = (0.1, 0.17333, 0.506666, −0.8, 3, 3, 1.4, 1.8), $i_1 = 0.066$, $i_2 = -0.56$, PP = (0.22, 0, −1, −1, 4, 4, 2, 2).

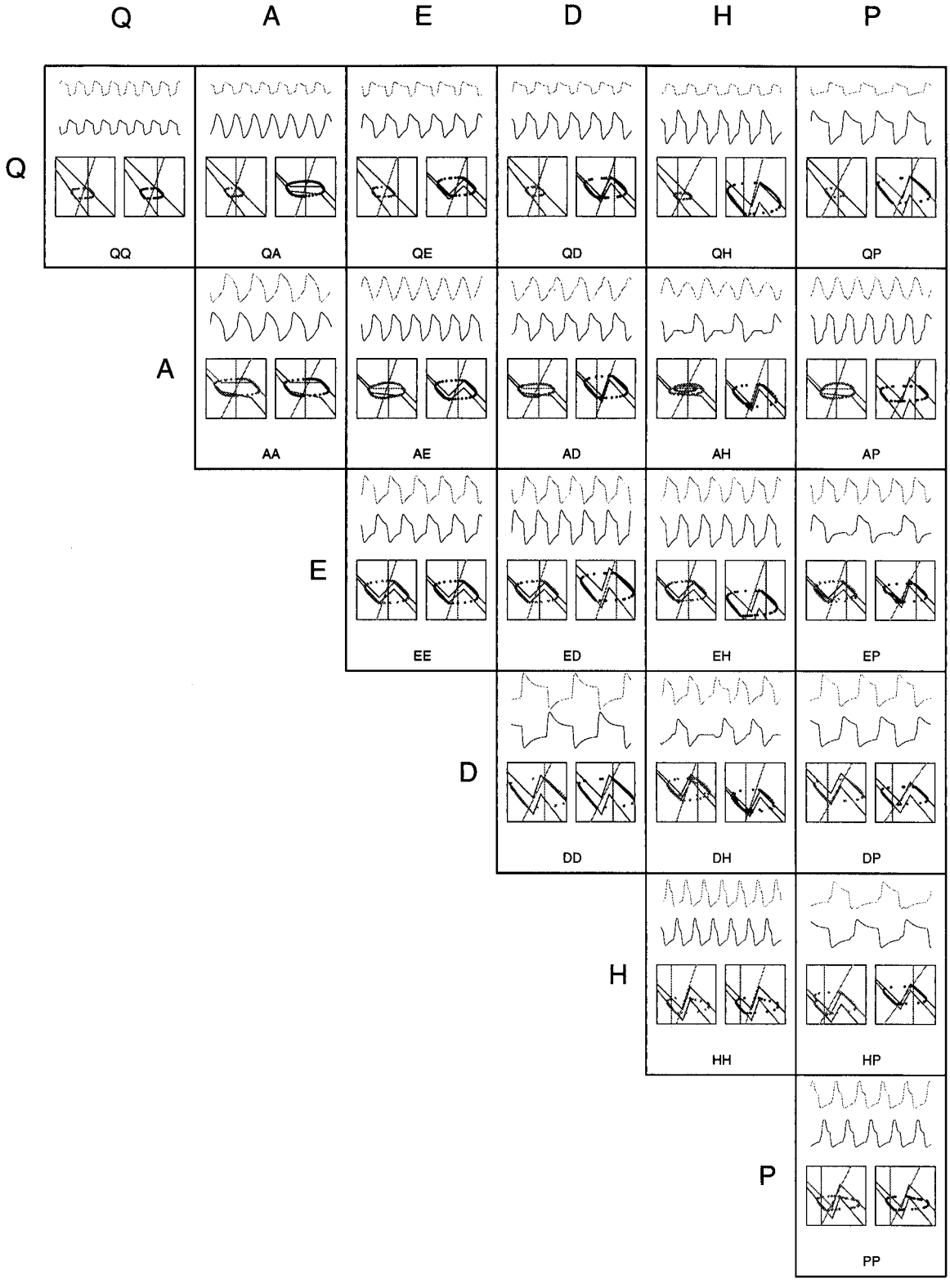
Q
A
E
D
H
P
QQ
QA
QE
QD
QH
QP
AA
AE
AD
AH
AP
EE
ED
EH
EP
DD
DH
DP
HH
HP
PP

is a summary figure showing antiphase oscillations being produced for each case.

In case EE, two identical endogenously oscillating cells linked with identical inhibitory synapses phase-lock exactly out of phase with each other, as to be expected. The positions of the synaptic thresholds have little effect, provided they lie between the maximum and minimum extent of each cell's potential. There is also an unstable in-phase solution. If the duty cycle of each cell is small, there is a stable in-phase solution (Kopell and Somers, 1995) that is not robust against perturbations. If the oscillators are not identical but have different intrinsic frequencies (by setting $\sigma_{s_1} \neq \sigma_{s_2}$),1:N and M:N phase-locking can occur.

In case AA, when each cell is already almost an oscillator, almost any inhibitory interaction will result in out-of-phase oscillations. So case AA is very similar to case EE. In the example shown in Fig. 7, each cell begins to spiral into a fixed point but is then perturbed slightly causing its state to move rapidly horizontally to the new position of the fast nullcline and then begin to spiral again.

The Case QQ: Two Quiescent Cells. If both cells are quiescent in isolation—that is, case QQ with $\sigma_f = 0$ in both cells—oscillations can still occur. The pair will oscillate provided the synaptic thresholds in each cell have the correct relationship to the fast and slow currents. In this case there are two distinct mechanisms of oscillation, *escape* and *release*.

When the presynaptic cell is below threshold ($V_{\text{pre}} < \theta$), the fast equation of the postsynaptic cell is

$$\tau_m \frac{\mathrm{d}V}{\mathrm{d}t} = -(V + q)$$

with fast nullcline

$$q = -V; \tag{16}$$

when the presynaptic cell is above threshold ($V_{\text{pre}} > \theta$), the fast equation is

$$\tau_m \frac{\mathrm{d}V}{\mathrm{d}t} = -(V + q + W(V - E_{\text{post}}))$$

with fast nullcline

$$q = -V(1 + W) + W E_{\text{post}}. \tag{17}$$

Thus, each cell has two fast nullclines, which we call the *free* and *inhibited* fast nullclines, defined by (16) and (17), respectively. In the phase portraits in Figs. 8 and 9, the diagonal lines from upper left to bottom right are the free (upper line) and inhibited (lower line) fast nullclines. Which one is in effect at any time depends on whether the potential of the other cell in the pair is above or below its threshold. When the cells are isolated, the phase portrait for each cell has two linear nullclines that intersect in a stable fixed point (Fig. 5a). When one of the cells is receiving inhibition, as in an inhibitory pair, the inhibited fast nullcline (Eq. (17)), intercepts the V-axis at

$$V = \frac{W}{1 + W} E_{\text{post}}, \text{ with slope } \quad -(1 + W).$$

Thus the effect of inhibitory synaptic input is to rotate the fast nullcline clockwise about the point $(E_{\text{post}}, -E_{\text{post}})$ by an angle $\tan^{-1}(-W)$. The new intersection points, I_1 and I_2, that define the rest potentials of the cells, are more negative than the points F_1, F_2 (Figs. 8 and 9).

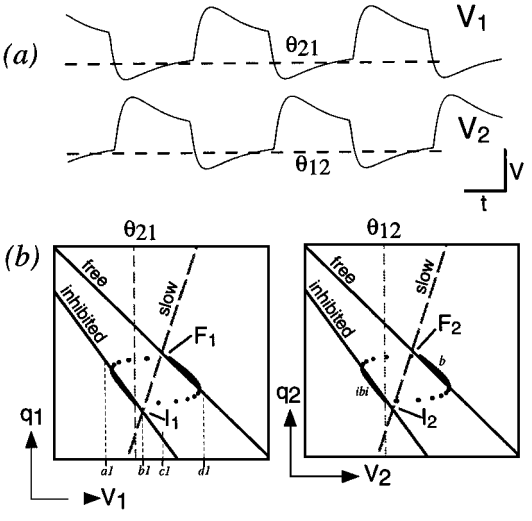

Figure 8. The escape mechanism for a pair of quiescent cells connected with reciprocal inhibition. (a) traces, (b) phase portraits. The vertical dashed line in each phase portrait is the threshold potential at which synaptic inhibition of the other cell begins. If the synaptic transfer function is sigmoid (Eq. (14)) and not a step function, the threshold line is at the half-height of the sigmoid curve. θ_{ij} is the presynaptic threshold for graded synaptic input from cell$_j$ to cell$_i$. In this and Figs. 9, 11, and 14, "slow" = slow (q-) nullcline, "free" = free fast (V-) nullcline, "inhibited" = inhibited fast (V-) nullcline, I_i is the inhibited fixed point and F_i is the free fixed point of cell$_i$, $i = 1, 2$. the "ibi" marks the interburst interval, "b" marks the burst interval, on the trajectory of cell$_2$. Parameters are, (0.4, 0.4, −0.5, −0.5, 0, 0, 3, 3).

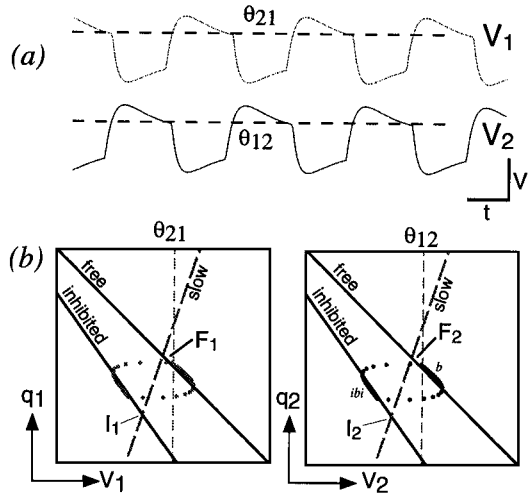

Figure 9. The release mechanism for a pair of quiescent cells connected with reciprocal inhibition. (a) traces, (b) phase portraits. Only the threshold position differentiates this figure from Fig. 8. Parameters are (0.4, 0.4, 0.2, 0.2, 0, 0, 3.3).

In these phase portraits, the point of intersection of a slow nullcline and a free fast nullcline is a *free* fixed posint (F_1 and F_2), and the point of intersection of a slow nullcline and an inhibited fast nullcline (I_1 and I_2), is an *inhibited* fixed point. When a cell is receiving no synaptic input, its state will either be at the free fixed point or will be moving slowly along the free nullcline toward it. When a cell is receiving inhibitory synaptic input, with a fixed postsynaptic conductance W, its state will either be at the inhibited fixed point or will be moving slowly along the inhibited fast nullcline toward it.

The Escape Mechanism. Suppose the synaptic thresholds θ_{21}, θ_{12} are below the potentials of the inhibited fixed points (I_1, I_2), respectively, as in Fig. 8. Now the pair of cells can oscillate as follows. Suppose cell_2 is above threshold and cell_1 is below threshold. This means that the state of cell_2 is moving slowly up along its free nullcline toward F_2 and the state of cell_1, currently to the left of the line $V_1 = \theta_{21}$, is on its inhibited nullcline and moving slowly down along it towards the fixed point I_1. Before the state of cell_1 reaches I_1, it crosses the threshold line $V_1 = \theta_{21}$, begins to inhibit cell_2, and causes the fast nullcline of cell_2 to immediately switch from the free to the inhibited position. Due to the difference in time constants (Eq. (3)), cell_2's state immediately follows the fast nullcline by moving rapidly left, approximately horizontally, toward the inhibited position of the fast nullcline. During this jump in position the potential of cell_2 descends below the threshold θ_{12} and thus cell_2 immediately stops inhibiting cell_1. The fast nullcline of cell_1 therefore switches from the inhibited to the free position so, similarly, the state of cell_1 jumps rapidly rightward to the new position of its fast nullcline, going above threshold θ_{21} in the process. By a three-stage process, cell_1 has "escaped from inhibition." Since cell_2 is below threshold, the cells have reversed their positions in the cycle. Now the same process, with cell_1 and cell_2 interchanged, occurs, so cell_2 also escapes from inhibition, beginning to inhibit cell_1: the cycle is complete.

The pair can be stationary with the states of the cells at the inhibited fixed points I_1 and I_2, because each cell is inhibiting the other. From this situation oscillations can be started by hyperpolarizing one of the cells below the synaptic threshold. This releases the other cell from inhibition and oscillations begin.

When the pair is oscillating, a small hyperpolarizing pulse will have little effect because it cannot cause a premature crossing of a threshold. A depolarizing pulse applied during a burst, when the state of the cell is on the free nullcline, will also have little effect, whereas the same pulse applied during the interburst interval can easily bring the potential above threshold, causing an early "escape from inhibition" if the pulse is not too short. Thus the pulse causes a phase advance in the two-cell network. In Fig. 8, right phase portrait, once can see that a depolarizing pulse during the trajectory segment *ibi* is the only reasonable way to cause a premature threshold crossing event.

Geometrically, the triangle formed by the slow nullcline, the inhibited fast nullcline, and the threshold $V_1 = \theta_{21}$ must lie to the left of the inhibited fixed point I_1 and not be too large. If θ is too negative, then the potential V will never reach it.

The Release Mechanism. Suppose that the thresholds of cell_1 and cell_2 are just above the potentials of the free fixed points F_1, F_2 respectively, as in Fig. 9. In this case the pair can oscillate by a similar mechanism. If the state of cell_1 is above threshold θ_{21} and the state of cell_2 is below threshold θ_{12}, the switch between cells is triggered by the state of cell_1, while being attracted toward the fixed point F_1, descending below threshold θ_{21} and thus releasing cell_2 from inhibition. The potential of cell_2 then jumps up, crossing threshold θ_{12} as it does so, and causes cell_1 to be inhibited. Now the situation of the cells has been reversed, and after cell_1 is

Table 1. Differences between the escape and release mechanisms for reciprocal inhibition between two quiescent cells.

	Escape	Release
Presynaptic threshold	Low	High
Fixed point	Both low	Both high
To start oscillation from rest	Hyperpolarizing pulse	Depolarizing pulse
To stop oscillations	Slow-tailed depolarizing pulse	Slow-tailed hyperpolarizing pulse
To advance pulse	Depolarizing pulse during interburst interval	Hyperpolarizing pulse during burst

released from inhibition by cell$_2$, one oscillation cycle is complete.

The pair can be stationary with the states of the cells at the free fixed points F_1 and F_2, because neither cell is inhibiting the other. Oscillations can be started by depolarizing one of the cells above the synaptic threshold. When the pair is oscillating, a depolarizing pulse has little effect because it cannot cause a premature crossing of a threshold. A hyperpolarizing pulse applied during an interburst interval, when the state of the cell is on the inhibited nullcline will also have little effect, but the same pulse applied during the burst will bring the potential below threshold prematurely, the cells will switch, the burst interval will be shortened, and the network is phase advanced. See trajectory segment *b* in Fig. 9. The different responses of the escape and release mechanisms to short pulses is summarized in Table 1.

Oscillations cannot occur if the threshold line in each phase portrait lies between the inhibited and free fixed points. This would occur if a neuromodulator either made the synaptic conductance W_{ij} too large or raised the synaptic threshold too high. One cell becomes locked at a high potential and the other cell at a low potential. The cells can switch (high $\leftrightarrow$ low) after application of a current pulse to one of the cells that causes it's membrane potential to cross the synaptic threshold (up or down). Thus each cell individually behaves as if it has intrinsic plateau potentials.

The relation between escape and release can be seen in the bifurcation diagram in the $W-\theta$ plane for the case QQ, Fig. 10. If the threshold is above the free rest potential—that is, the V-coordinate of the free fixed point F_i,—but not too high, then oscillations by release occur (region OR-SS$_{FF}$). Oscillations by escape occur for threshold in a relatively narrow band of negative values (region OE-SS$_{II}$). Otherwise the pair does not oscillate. Note the region of plateau potentials when the synaptic threshold lies between the values required

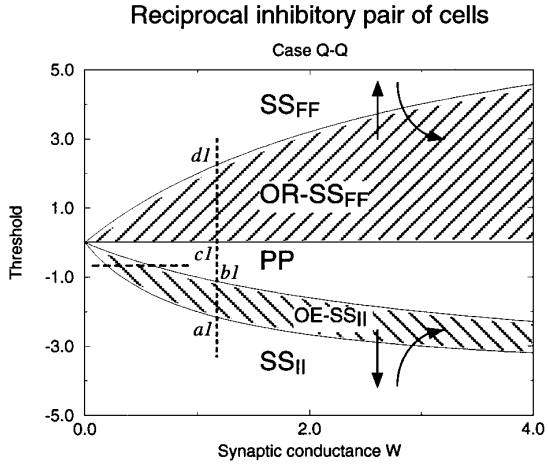

Figure 10. Bifurcation diagram for two quiescent cells connected with symmetrical reciprocal inhibition (case QQ), in the $W-\theta$ plane. Note that the θ-axis could be replaced by an equivalent injected current axis (with different scale). See text. Model parameters as for Figs. 8 and 9. The five regions are: SS$_{FF}$, steady-state at (F_1, F_2); OR-SS$_{FF}$, oscillations by release or steady-state at (F_1, F_2); PP, plateau potentials where the two steady states are (I_1, F_2) or (F_1, I_2); OE-SS$_{II}I$, oscillations by escape or steady-state at (I_1, I_2); SS$_{II}$, steady-state ate (I_1, I_2). The arrows across the OR-SS$_{FF}$-SS$_{FF}$ border indicate that oscillations by release could be stopped by shifting the threshold upwards—thus destroying oscillations by release if present—and then slowly moving the threshold back to its original value. Equivalently, by the same effect can be obtained by injecting and slowly releasing a hyperpolarizing current. Similarly, the arrows across the OE-SS$_{II}I$-SS$_{II}$ border indicate that oscillations by escape could be stopped by shifting the threshold downwards and slowly returning to its original value, or equivalently, by injecting and slowly releasing a depolarizing current. The points a_1, b_1, c_1, d_1 on the vertical dotted line are defined by corresponding labeled points in Fig. 8(b).

for escape and release. Here, either one cell is free and inhibiting the other cell, or vice versa, and small pulses to one of the cells can cause the pair to switch polarities like a flip-flop. However, this region reduces in size and disappears when the gain of the synaptic transmission function (γ) is sufficiently reduced.

Thus the presence of plateau-like responses in a non-isolated cell does not necessarily imply these are caused by intracellular mechanisms but may rather be caused by network interactions. The dashed line shows that if the synaptic conductance W could be slowly increased, keeping the synaptic threshold below rest, then the pair would change from a state in which both cells are inhibited, to oscillations by escape, to network plateau potentials.

One can see that if the threshold for graded synaptic transmission could be changed one would traverse (from low to high threshold) the following range of behaviors: steady-state with each cell inhibiting the other (region SS_{II}); either oscillations by escape or a steady-state with each cell inhibiting the other (region OE-SS_{II}); plateau potentials with switches between which cell is free and inhibiting the other (region PP); either oscillations by release steady-state with both cells free of inhibition (region OR-SS_{FF}); and steady-state with both cells below threshold, free of inhibition (region SS_{FF}).

A Duality Between Threshold and Injected Current. There is an approximate duality between the presynaptic threshold for graded transmission (*graded threshold*) and the amount of injected current, for the following reason. An injected current shifts the fast—free and inhibited—nullclines up (depolarizing current) or down (hyperpolarizing), without shifting the slow nullcline. Consider Fig. 9, left panel. A depolarizing current injection shifts the fast nullclines toward less negative potentials, causing the fixed points F_1 and I_1 to move rightward in the phase plane. Thus such a current raises the fixed points to less negative potentials. The first major change occurs when the fixed points bracket the graded threshold—with the possibility of plateau potentials. When more depolarizing current is applied the fixed point I_1 would lie above the graded threshold, in position for oscillations using the escape mechanism. Now the phase portraits of Fig. 8 describe the dynamics of these oscillations. Here one can see that shifting the threshold to lie below (more negative than) the potential labeled $a1$ would destroy this mechanism. Translating to currents, even more depolarizing current in each cell would cause the difference in potential between the fixed points (F_1, I_1, F_2, I_2) and the threshold to be too large for the threshold-crossing events needed for the escape mechanism to occur; consequently the pair of cells will approach a steady-state with each cell inhibiting and being inhibited by the other (region SS_{II}).

By the preceding description one can use current injections to get a change in behavior almost the same as that obtained by shifting the graded threshold. The only differences between a behavior change obtained by modifying the graded threshold and that obtained by injecting a current are: (1) the ranges of the oscillations in each case will be different, since the fixed points are shifted along the voltage axis; and (2) the frequencies of the oscillations will be slightly different because of the spreading apart of free and inhibited fast nullclines with depolarizing current that affects the amount of time spent on the slow parts of the limit cycle.

An important caveat must be added. This duality between moving a threshold and altering the injected current applies only over ranges of membrane potential for which the fast nullclines are approximately linear—that is, the fast IV curve, with and without synaptic current, must be approximately linear in the range considered.

Generally, the graded threshold is fixed in an experiment, but this approximate duality allows for the changing of behaviors, and hence mechanisms of oscillation, by using injected currents instead to obtain the same effects. For example, the series of behaviors corresponding to regions SS_{II}, OE-SS_{II}, PP, OR-SS_{FF}, SS_{FF}, would be obtained, if one started in SS_{II}, by injecting successively larger a mounts of hyperpolarizing current into both cells.

In the leech, reciprocal inhibitory pairs of heart interneurons are believed to oscillate by an escape mechanism (Calabrese et al., 1995). The swim CPG in *Clione* (Arshavsky et al., 1985a, b, c, d) appears to operate by a release mechanism. In the isolated lobster stomatogastric ganglion, with no extraganglion modulatory inputs, the cells LP and PD in the pyloric CPG appear to oscillate by an escape mechanism (Miller and Selverston, 1982).

Case PP: Both Cells Have Plateau Potentials. This is illustrated in Fig. 11. When there are no synaptic inputs, cell_1 has two fixed points, H_1 and D_1, and cell_2 has fixed points H_2 and D_2. Brief current pulses applied to cell_1 can cause its potential to jump between H_1 and D_1. Similarly, brief current pulses applied to cell_2 can cause jumps between H_2 and D_2. The synaptic strengths must be large enough to destroy the high plateau fixed points D_1 and D_2.

When cell_1 is receiving inhibitory synaptic input from cell_2, the fast nullcline shifts to its inhibited position by a downward motion and a small clockwise

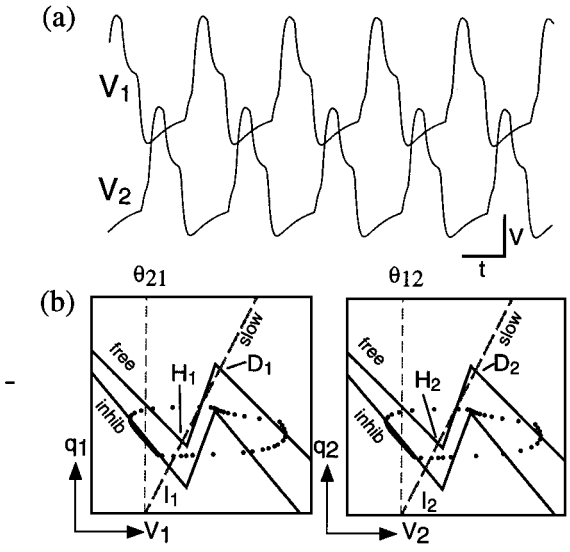

Figure 11. Two cells, each exhibiting plateau potentials, may oscillate when linked with reciprocal inhibition, in this case by an escape mechanism. (a) traces, (b) phase portraits. ("slow," "free," "inhibited" as in Fig. 8). The slow nullcline in each cell intersects the fast nullcline in three places; the points H_i and D_i are the low and high plateau potentials in cell$_i$, $i = 1, 2$. Parameters are $(0.2, -1, -1, 4, 4, 2, 2)$.

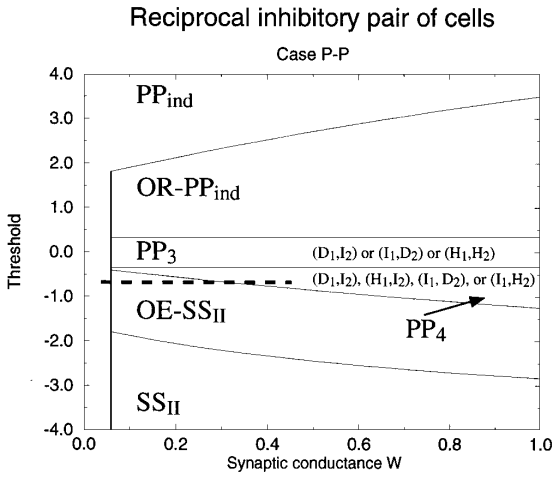

Figure 12. Bifurcation diagram for two cells with plateau potentials when connected with symmetrical reciprocal inhibition (case PP), in the W-θ plane. Other parameters as in Fig. 11. The six regions are: PP$_{\text{ind}}$, each cell is at a Plateau potential (l_i or D_i) independently of the other cell; OR-PP$_{\text{ind}}$, oscillations by release or a steady state with each cell at independent plateau potentials; PP$_3$, three possible steady states—(H_1, I_2), (L_1, H_2) or (H_1, H_2); PP$_4$, four possible steady states—(H_1, I_2), (L_1, I_2), (l_1, H_2) or (I_1, L_2); OE-SS$_{\text{II}}$, oscillations by escape or steady-state at (I_1, I_2); SS$_{\text{II}}$, steady-state at $(I_1, I_2.)$

rotation, resulting in a single inhibitory fixed point I_1. Similarly, cell$_2$ has the single inhibited fixed point I_2. In the situation in Fig. 11, the synaptic threshold for each cell is below the potential of the cell's inhibited fixed point. If cell$_1$'s potential is below threshold and cell$_2$'s potential above threshold, the state of cell$_1$ moves rapidly onto the inhibited fast nullcline and begins to move slowly along it toward I_1, while the state of cell$_2$ is attracted onto the free nullcline and moves up toward the high free fixed point D_2. Since θ_{21} is so low, the state of cell$_1$ stays below threshold only briefly then crosses θ_{21}, inhibits cell$_2$, and causes the inhibited fast nullcline to come into effect there. The state of cell$_2$ moves rapidly left onto the left leg of the inhibited fast nullcline. Before reaching the inhibited fast nullcline the state goes below threshold θ_{12}, finally allowing the state of cell$_1$ rebound up to the right leg of cell$_1$'s free fast nullcline. Now a situation has bee reached with cell$_1$ depolarized above threshold and cell$_2$ hyperpolarized below threshold, so the same mechanism with the cells interchanged will bring the system back to the starting state, and one cycle is complete. This process is closely related to the escape mechanism for a pair of quiescent cells. Similarly, two cells with plateau potentials can also oscillate through a release mechanism.

The downward and upward shoulders in the traces are due to the slowing of the trajectories near the upward knee in the free nullcline and the downward knee in the inhibited nullcline.

If the graded thresholds are fixed at a potential more negative than the rest potential (see dashed line in Fig. 12), then there is a window of synaptic strengths ($W_{12} = W_{21}$) for which oscillations can occur. If W is too small, the high fixed point still exists on the inhibited free nullcline so oscillations do not occur, and if W is too large, then the intersection points I_i are to the left of the thresholds θ_{ij} and the pair locks up with one cell's state at I_i and the other at D_j. If the graded thresholds are at potential significantly more positive than the rest potential (such as 1.0 in Fig. 12), then oscillations by release occur for all synaptic strengths above a minimum value.

The bifurcation diagram for case PP, Fig. 12, is similar to the bifurcation diagram for case QQ, but with a positive minimum synaptic conductance W sufficient to destroy D_i (vertical line on left) and also a minimum positive threshold for oscillation by release. This threshold is the potential of the high fixed point D.

Case DQ: One Cell Depolarized, One Quiescent. This case, in Fig. 13, demonstrates the difference between

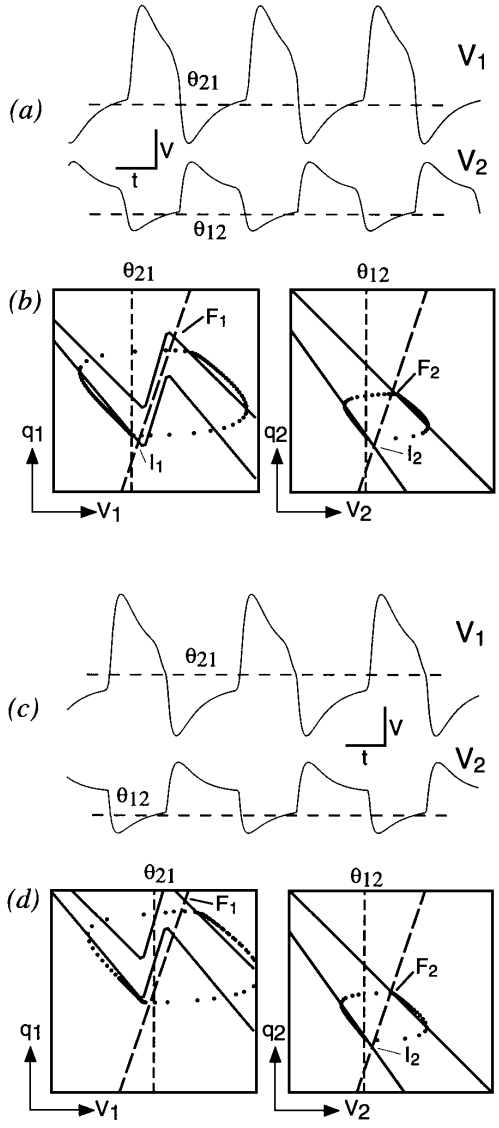

Figure 13. The synaptic and intrinsic escape mechanism. (a) and (b), oscillations by synaptic escape; (c) and (d), oscillations by intrinsic escape. Nullcline labels have been omitted. Note the difference in the cell_1 phase portrait in (b) and (d). There is no inhibited fixed point I_1 in (d) and the threshold is higher (less negative) in (d) than in (c). Parameters are, synaptic, (0.2, 0.4, −0.466, −0.52, 4. 5, 0, 3, 3), $i_1 = 0.4$, $i_2 = 0$, intrinsic, (0.2, 0.4, 0, −0.466, −0.52, 4.5, 0, 3, 3), $i_1 = 1.38$, $i_2 = 0$.

synaptic and *intrinsic* mechanisms as introduced by Skinner et al. (1994). Another instance using a release mechanism appears in Fig. 7, QD. The oscillations in the top two panels show oscillations by synaptic escape in both cells, while in the bottom two panels oscillations by escape are again present, but by intrinsic escape in cell_1 and by synaptic escape in cell_2. In the latter case, cell_1 escapes from inhibition simply by coming to the downward knee in the inhibited nullcline and jumping onto the right branch of the free nullcline, crossing threshold as it does so. In moving from the (ab) case to the (cd) case, more depolarizing current is present in cell_1 and its graded threshold has been made less negative. This shift in threshold could not be achieved by suitable current injections as described earlier when the fast nullclines are completely linear. One could achieve the same effect as this threshold shift if it were possible to lower (make more negative) the reversal potential for the lumped fast IV curve.

The Remaining Cases. The other five cases where both cells of the pair have N-shaped fast nullclines, but neither cell is an endogenous oscillator (cases HP, DP, HH, DH, DD), are very similar to the PP case, and we will not describe them in detail. The DH example in Fig. 7 shows cell_1 "missing a beat" to give 1 : 2 frequency locking. The mechanisms at work in case DH and in the 2 : 1 frequency locking examples of cases EP and AH have one component in common, which we will discuss after describing the 1 : 4 frequency locking case shown in Fig. 14.

In the case QE shown, the threshold in cell_1 is too high so the cell is being driven by cell_2 with no feedback. In cases QD, QH, and QA the Q cell acts as a switch that keeps the second cell oscillating, essentially by injecting current pulses into the second cell, resulting in responses like those shown in Figs. 5d, e, and b, respectively. In the A row, AE, AD, AH, and AP, the position of the first cell's threshold does not need to be set carefully so long as it lies within the upper and lower extremes of the membrane potential. In the E row, again the threshold of the first cell does not need to be set carefully. In case DD, the thresholds are in the release position very close to the depolarized rest potential, thus extending the length of the burst and reducing the frequency.

1:N Frequency Locking. In the pair of cells in Fig. 14, cell_2 would be an endogenous oscillator if isolated since the slow nullcline intersects the fast nullcline at a single point between the two knees of the fast nullcline. Cell_1 has a split slow current with a significantly smaller inward conductance than the outward conductance. Thus the slow nullcline intersects the free fast nullcline at a single point, F_1. So if cell_1 was isolated, its state would remain at the fixed point F_1. If cell_1

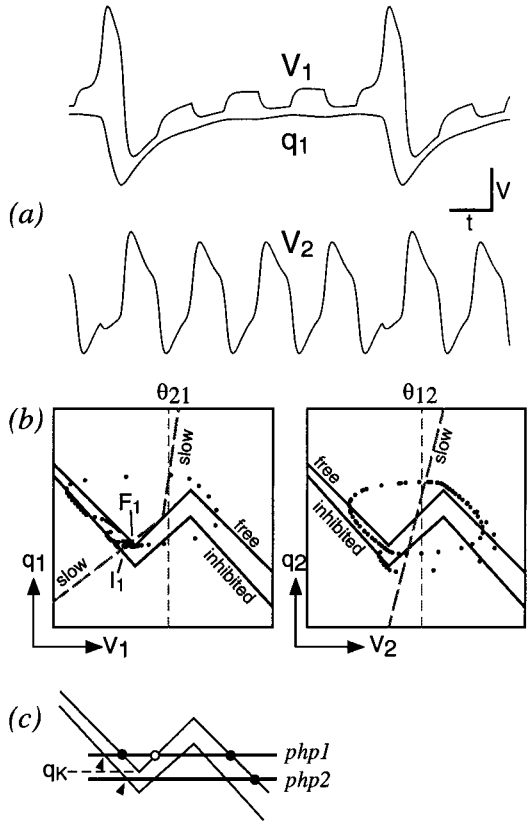

Figure 14. 1 : 4 frequency locking in a pair of cells connected with reciprocal inhibition. (a) Traces of V_1, q_1, and V_2. The q_1 trace has been inverted to show similarity to the I_h conductance in the E-cell model of Kopell and LeMasson (1994), the H activation variables of Wang (1994), and the (Wang et al., 1995) I_h current in TC cells. (b) Phase portraits—"slow," "free," and "inhibited" as in Fig. 8. There are no stable fixed points in cell_2. Parameters are (0.106667, 0.106667, 0.1, 0.1, 2, 2, (0.76666, 7.1), 4). Note the pair of conductances $(\sigma_{\text{in}}, \sigma_{\text{out}})$ given for the split slow current in cell_1. (c) Schema showing detail of the one-dimensional phase-portraits at the left "knee" in the V-nullcline of cell_1. If cell_1 is being inhibited by cell_2 and than released at the first arrowhead on the inhibited V-nullcline, the horizontal movement is defined by the one-dimensional phase portrait *php*1 so the state jumps only to the left fixed point. If cell_1 is released at the second arrowhead, the one-dimensional phase portrait has only one fixed point so the state jumps to the right leg of the free nullcline.

receives a constant depolarizing current, enough that the free fast nullcline intersects the slow nullcline in a single point between the two knees of the fast nullcline, it becomes an endogenous oscillator with a duty cycle of less than one half.

When the cells are linked with reciprocal inhibition, cell_2 continues to oscillate in manner very similar to the isolated condition. This holds true only if the synaptic connection strength W_{21} does not move the point of intersection of the inhibited and slow nullclines outside the region between the knees of the inhibited fast nullcline. Then cell_2 will continue to oscillate whether cell_1 is above or below threshold. When cell_1 is hyperpolarized by cell_2, its free fast nullcline shifts to an inhibited position (see left phase portrait in Fig. 14) which intersects the slow nullcline at the inhibited fixed point I_1. Suppose for the moment that cell_1 is permanently inhibited by cell_2. The state of cell_1 travels slowly down the inhibited fast nullcline toward I_1, moving more slowly the closer it gets. Let q_K be the q-coordinate of the downward-pointing knee of the free fast nullcline. Since the q-coordinate of I_1 is below q_K, eventually the state of cell_1 will get so close to I_1 that its q-coordinate is below q_K. If at this time inhibition by cell_2 is removed, cell_1's state will rebound and jump onto the right leg of the free nullcline. At this moment the horizontal line through the state of cell_1 defines a one-dimensional phase-portrait with a single attracting fixed point at the intersection of the right leg of the free fast nullcline with the horizontal line. If the inhibition by cell_2 is removed too early, with the q-coordinate of the state still above q_K, the one-dimensional phase-portrait defined on the horizontal line through the state still has three fixed points. See Fig. 14(c), *php*1 and *php*2. In particular the left leg of the free fast nullcline defines an attracting fixed point on this one-dimensional phase-portrait so the state of cell_1 jumps only a short distance onto the left leg of the free fast nullcline, and then moves slowly down the free fast nullcline toward the free fixed point F_1. If the inhibition by cell_2 is restarted, the state will switch back onto the left leg of the inhibited fast nullcline and continue moving slowly downward, this time toward I_1. Thus the left legs of the free and inhibited fast nullclines define two sides of a corridor down which the state of cell_1 moves, sometimes on one side towards F_1, sometimes on the other toward F_2, depending on whether cell_2 is inhibiting cell_1 or not.

Since cell_2 continues to oscillate whatever the state of cell_1, eventually the state of cell_1 gets low enough—below q_K—that the next time cell_1 is released from inhibition by cell_2, its state jumps right all the way onto the right leg of the free fast nullcline. However, since the q-distance between I_1 and the downward-pointing knee of the free fast nullcline is small, the state passes very close to this knee while jumping right. This slows down the jump (cf. Eq. (9)), causing the

pronounced shoulder in the membrane potential trace of cell_1 as it rises to the single main peak in each cycle. The three intermediate bumps between each main peak correspond to the trapping of the cell_1 state on the right side of the corridor when the inhibition from cell_2 is removed.

The potential of cell_2 continues to oscillate endogenously while the state of cell_1 is below threshold. When the cell_1 state finally escapes from the corridor and jumps to the right leg of its free fast nullcline, it rises above threshold, causing the state of cell_2 to be confined for a brief time to its inhibited free nullcline. This can be seen in cell_2's trajectory where it switches from the left leg of the free fast nullcline to the left leg of the inhibited fast nullcline. By the time the cell_2 state begins to jump right, the state of cell_1 has gone below threshold again, so the cell_2 free fast nullcline is reinstated. This can be seen as the lower trajectory in the cell_2 phase-portrait and also as the small downward step in the V_2 membrane potential trace. Immediately following this step the rate of movement along the inhibited fast nullcline is slower than along the free fast nullcline because in the phase-portrait the distance between the state and the slow nullcline is less (cf. Eq. (10)); hence the slope of cell_2's potential trace is smaller immediately after the step than just before it. The cell_2 potential then rebounds into a higher peak than the previous three cycles.

In Fig. 7, the cases EP, AH, and DH all involve essentially the same mechanism: the state is trapped between the left legs of the free and inhibited positions of the fast nullcline until it gets low enough that after the next release from inhibition the state can rebound up to the right-leg of the fast nullcline. The fine details vary from case to case and the careful reader will easily work them out.

4. Discussion

In this paper we provided a tutorial introduction to one- and two-dimensional phase portraits, introduced a simple two-dimensional cell model, and used it to analyze dynamical mechanisms underlying oscillations by a pair of cells connected with fast reciprocal inhibition. The answer to the original question—whether, in order for an arbitrary pair of cells connected with reciprocal inhibitory synapses to oscillate, any other mechanism besides release and escape need be considered—is a disappointing no when the synapses are fast and the gain γ of the synaptic transfer function is high.

Different pairs of cellular types oscillate by different dynamical mechanisms. If both cells are oscillators, then obviously the reciprocal inhibitory pair will oscillate; the synaptic connections provide a mechanism for the oscillators to phase-lock in a specific relative phase. When the natural frequency of each cell is different (due to different σ_s values), the phase of each cell relative to the other is shifted slightly so that the cells are no longer exactly 180° out of phase. If only one cell is an oscillator, the oscillating cell drives the reciprocal inhibitory pair and the other cell is a follower. If neither cell is an oscillator, in particular if each cell is completely quiescent, then some other mechanism is needed. Here we have shown how oscillations can arise in a reciprocal inhibitory pair of individually quiescent cells by means of escape or release mechanisms. The same cell model allows us to construct a model of $1:N$ frequency locking in the reciprocal inhibitory pair that relies on a dynamics where the phase point of one cell gets "trapped" between the free and inhibited positions of this cell's fast nullcline for several cycles of the other cell. This same mechanism can give rise to $1:N$ frequency locking in several different pairs of reciprocal inhibitory pairs, such as, cases EP, AH, and DH in Fig. 7.

4.1. *Usefulness of Geometrical Description*

We have shown how to use the geometric properties of phase portraits to understand the dynamic properties of a simple cell model and of the reciprocal inhibitory pair of neurons. The cell model was originally derived to match the major dynamical properties of stomatogastric ganglion neurons, such as postinhibitory rebound, plateau potentials, and endogenous oscillations. When two such models are combined by graded inhibition into a four-dimensional model of reciprocal inhibition using fast synapses, the resulting dynamical behavior can be analyzed using geometrical relationships between phase planes. This approach to modeling single cells depends critically on the existence of a significant difference in time scales between the "fast" currents and the "slow" currents.

4.2. *Behavioral Range of the Cell Model*

The cell model displays behaviors corresponding to physiological properties of individual neurons such as endogenous oscillations, postinhibitory rebound in an otherwise quiescent cell, plateau potentials, tonic

firing, or chronic hyperpolarization. Six different behaviors of an isolated cell can be characterized by geometrical properties in the cell's phase portrait (Fig. 5) These properties in turn translate into geometrical relationships between the IV curves of the lumped fast and slow currents.

4.3. Behavioral Range of the Model of Reciprocal Inhibition

Our cell model enabled us to explain how every combination of individual cellular behaviors can generate oscillations in the reciprocal inhibitory pair and provides a unified explanation of many different IP behaviors. It shows how a cell that exhibits endogenous plateau potentials but not endogenous oscillations can be part of the pattern-generating mechanism when linked to another cell with plateau potentials or even to a quiescent cell, provided the synaptic strengths and thresholds are within the correct ranges. On the other hand, when a nonisolated cell displays plateau potentials, it is possible that these are caused by synaptic interactions with another cell, not by an endogenous mechanism, as shown by the bifurcation diagrams Figs. 10 and 12. The basic mechanisms involved in all cases when neither cell is an oscillator are escape and release.

4.4. Physiological Ranges of Synaptic Threshold and Conductance

In this review we have seen that the mechanisms of oscillation when neither cell is an oscillator depend critically on relationships between the presynaptic threshold for postsynaptic activation, the synaptic strength, and the IV curve for the slow current. Further, these relationships vary from one mechanism to another. Thus it is appropriate to ask for the physiologically appropriate ranges for synaptic threshold and synaptic strength in a specific system such as the lobster gastric mill CPG. The synaptic threshold for graded transmission in the lobster gastric mill has been measured at ≈ -47 mV (Graubard, 1978; Johnson et al., 1991) and as ≈ -59 mV (Graubard et al 1983). Release thresholds in other systems range from ≈ -40 mV to ≈ -75 mV (Harris-Warrick et al., 1992b, p. 79).

The postsynaptic conductance (strength) has rarely, if ever, been measured directly. A rough measure of the relative strength of several gastric mill synapses, in one neuromodulatory condition, was obtained by Russell (1985) by measuring the change in postsynaptic firing rate in response to a change in firing rate of the presynaptic cell. In a different neuromodulatory condition (the gastric and pyloric CPGs are in the same ganglion) the relative strengths of the pyloric synapses was measured by Miller and Selverston (1982) by a similar method. Exact figures for the conductances associated with these synapses are not known. Data on the relative efficacy of stomatogastric ganglion synapses was summarized by Wiens (1982). In a modeling study of the leech heart CPG, that contains a small network of identified neurons, Nadim et al., (1995) used a value of 300 nS for the graded postsynaptic conductance.

Two examples of the appropriate ranges for connection strength and threshold, for the two cases QQ and PP, are given in Figs. 10 and 12. In order to map the range thus derived into physiological units, one has to assume a physiological, presumably conductance-based, model and derive a mapping between the units used here in our semiconductance-based model and the conductance-based model. An approximate mapping is derived in the Appendix between the model used throughout this review and the Morris-LeCar model (1981).

4.5. Plateau Potentials

Plateau potentials are important in generating motor behavior (Marder, 1991; Kiehn, 1991). From Fig. 6 we see that once the gain of the fast inward current is above a certain threshold, an isolated cell will have plateau potentials, and that a steady current injection will convert it into a steady depolarized or hyperpolarized states. From Fig. 10 we see that even if an individual cell does not possess plateau potentials, the same cell embedded in a network connected with graded synaptic transmission could have plateau potentials and that, once established, plateau potentials are insensitive to synaptic strength. However, if the gain of the synaptic transfer function is low enough that the width of the sigmoid is a significant proportion of the potential difference between the free and inhibited fixed points, the region of plateau potentials in this figure disappears for low synaptic conductance. We also see from this diagram that a change in threshold in a nonisolated cell, hence a current injection (cf. Fig. 10), can convert plateau potentials into oscillatory behavior. This may be the reason why plateau potentials have often been confused with oscillatory behavior in the past (Marder, 1991).

4.6. Effect of Slow Synapses

When the synaptic time course is comparable with the cycle time, other behaviors than out of phase oscillations are possible for the reciprocal inhibitory pair. In particular synchronous oscillations are possible. This was first shown by Wang and Rinzel (1992) in a model with slow graded synaptic transmission, and subsequently Van Vreeswijk et al. (1994) elegantly showed that when spike-mediated transmission is used, synchronous oscillations are to be expected when the rise time of the synaptic response is longer than the duration of an action potential. Hansel et al. (1995) considered networks connected with excitatory synapses and showed that in general, excitatory synapses with a slow time course cause pairs of cells to be desynchronized. The same arguments applied to inhibitory synapses show that pairs will become synchronized. Wang and Rinzel (1993) applied their 1992 model to investigate sleep spindle rhythmicity in thalamic nuclei. Because $GABA_B$ receptors mediate inhibition with a large delay constant, their model suggests that $GABA_B$ receptors may play a critical role in synchronization among reticular neurons.

4.7. Comparison with Other Work

Our survey extends and complements the work of Wang and Rinzel (1992) and Skinner et al. (1994). Our model's dynamical behavior is similar to the conductance-based Morris-Lecar model (Morris and Lecar, 1981) used by Skinner et al. (1994), and LoFaro et al. (1994) to study reciprocal inhibition, and by Somers and Kopell (1993) and Kopell and Somers (1995) to study mutual excitation. The latter authors explored why two Morris-LeCar cells linked with mutual excitation will approach complete synchrony very rapidly, essentially within one cycle, and stated conditions on the dynamics of any two-dimensional cell model for this to occur. Termed *compression*, these conditions are also satisfied by our cell model. The arguments for synchronization of mutually excitatory cells apply equally well to antiphase oscillations of reciprocally inhibitory cells. For this reason our model reciprocal inhibitory pairs always converge to antiphases of behavior very rapidly, within one cycle. In a second paper (Kopell and Somers, 1995) they pointed out that, although synchronous oscillations are always possible with mutual excitation, antisynchronous oscillations can also occur provided a further restriction is satisfied. A pre-requisite for this restriction to hold is that the duty-cycle of the oscillators is small. However, small perturbations to the antisynchronous oscillation usually result in it being replaced by the synchronous oscillation, so it is not clear whether this additional oscillation mode will be of biological significance. Our model and the Morris-LeCar model both satisfy the extra Kopell-Somers restriction when the duty cycle is small, and thus, when reciprocal inhibition is considered, one finds a second oscillation mode that is synchronous. However, the rate of approach to the secondary oscillation mode is much slower than to the first, and when the mode is established it is not robust to small perturbations.

Escape and release mechanisms have been previously described by (Wang and Rinzel, 1992). Their cell model includes a leak current and a voltage dependent inward current that activates instantaneously and inactivates slowly. The fast nullcline arising from their current equation corresponds to our fast nullcline, and the nullcline arising from the equation for inactivation of the inward current corresponds to our slow nullcline. Their nullclines intersect at single points when the fast nullcline is either free or inhibited; the rebound excitation when the other cell falls below synaptic threshold gives rise to oscillations. The abstract dynamical mechanism is the same in their model and in ours, when considered as properties of linked phase-portraits, but the physiological implementations of the mechanisms differ: in their case the slow variable controls inactivation of the conductance of an inward current, while in our model the slow variable controls the activation of a current.

Rose and Hindmarsh (1989a, 1989b, 1989c) and Hindmarsh and Rose (1994a, 1989b, 1989c) make extensive use of phase diagrams in providing a deep analysis of the properties of thalamo-cortical neurons. In particular, at one point they use a "lumped slow current" in reducing a six-dimensional model to a two-dimensional model; most of their analyses are dependent on geometric properties in a two dimensional phase plane.

4.8. 1:N Frequency Locking

A $1:N$ frequency-locking mechanism was described by LoFaro et al. (1994) and Wang (1994). LoFaro et al. (1994) used a model reciprocal inhibitory pair using the Morris-Lecar equations for each cell with the addition of a slow inward i_h-like current in one cell, and

a synaptic model similar to ours except that in some cases the synaptic current had a time-dependent, but fast, build-up. In their model, the frequency-locking ratio increased as the hyperpolarizing current injected into the i_h-cell in creased (LoFaro et al., 1994, Fig. 2), in agreement with data from the pyloric CPG in the lobster. We obtain almost identical behavior in our model: a depolarizing current of appropriate amplitude in cell_1 raises its fast nullcline (Fig. 14), so that 1 : 1 frequency-locking occurs. Then as this is reduced, or equivalently, as hyperpolarizing current is increased, the ratio changes to 1 : 2 to 1 : 3 to 1 : 4. Higher ratios also occur (data not shown). The details of the mechanisms differ slightly because the (LoFaro et al., 1994) model has a slow potassium current and, in addition, a third equation for an i_h current; the latter serves to slowly shift the position of the fast nullcline and hence the position of the inhibited fixed point (cf. the fixed point I_1 in Fig. 14). We used a reduced conductance for the inward portion of the slow current, obtaining the same behavior with only a two-equation model for cell_1. We can also obtain this behavior by keeping the same conductance for the inward and outward parts of the slow current but making the time constant for the inward part slower.

Wang (1994) studied two dynamical modes of a four-dimensional model of a thalamic relay neuron with six ionic currents. In addition to an I_h-current, his model had I_T, I_{Na}, I_K, I_{NaP}, and I_L currents. One mode was rhythmic bursting in response to steady injected current, the other was intermittent phase-locking when driven by a periodic hyperpolarizing current injection. Both these behaviors occur in simple form in our model (Fig. 14): if the feedback inhibition from cell_2 is removed and a depolarizing current injected, cell_1 exhibits bursting; other wise $1 : N$ intermittent phase-locking occurs as described. A wide variety of intermittent phase-locking phenomena were found to occur, including the case of $1 : N$ of a phase-locking for $N = 2, 3, 5, 6$. One conclusion was that the intermittent phase-locking originated from a temporal integration of hyperpolarizations by the slowly activating sag current I_h. The activation variable H for the I_h current displays a similar time-course to our slow current variable q_1 (Fig. 14(a)), which has been inverted in the figure to show the similarity.

Thus our model for $1 : N$ frequency locking between two cells (Fig. 14) contains the essential ingredients underlying the mechanisms of LoFaro et al. (1994) and of Wang (1994). Kopell and LeMasson (1994) and Wang et al. (1995) both went further and used a distributed versions of this mechanism in large networks, the former as a model of cortical architecture, and the latter as a component mechanism in a large-scale thalamic network model with two cell populations: the excitatory thalamocortical (TC) relay neurons and the inhibitory nucleus reticularis thalami (RE) neurons. Cell_1 in Fig. 14 maps to the TC cells and cell_2 maps to the RE neurons. In the network model of Kopell and LeMasson (1994), their E cells burst intermittently and have a slow inward I_h type current for which the conductance has a time course that is similar to the time course of the slow current in cell_1, plotted as $-q_1$ in Fig. 14.

4.9. Neuromodulators

The motor patterns produced by a CPG such as the lobster gastric mill can be profoundly altered by numerous neuromodulatory substances, for example acetylcholine, dopamine, histamine, proctolin, octopamine, serotonin (see Selverston, 1993, for a review). Changes in synaptic efficacy—but not in synaptic conductance—at all pyloric synapses in response to the neuromodulators dopamine, serotonin and octopamine was investigated by Harris-Warrick et al. (1992a) (summarized in Harris-Warrick et al., 1992b). In a few cases, some biophysical changes underlying neuromodulator-induced behavioral changes are known; one is the effect of dopamine on the lobster pyloric CPG. The numerous biophysical changes underlying the behavioral effects of dopamine (Harris-Warrick and Marder, 1991) include (1) reduction of amount of transmitter release by the PD cell (Eisen and Marder, 1984), (2) reduction in the transient K^+ current I_A in the PY neurons (Harris-Warrick et al., 1995b), (3) modulation of the I_A and I_h currents in the LP cell (Harris-Warrick et al., 1995a). Dopamine modulated I_A by reducing its maximal conductance and shifting its activation and inactivation curves, while it modulated I_h by shifting its activation curve in the depolarized direction and increasing its gain. In the case of serotonin, the biophysical effects on one crustacean motoneurone were measured by Kiehn and Harris-Warrick (1992): serotonin enhances I_h and decreases $I_{K(Ca)}$.

4.10. Final Summary

We have shown that when attention is restricted to a very simple two-dimensional dynamical cell model,

the mechanisms of escape and release are sufficient to produce oscillatory behavior in essentially all cases of reciprocal inhibition. We have also provided a parsimonious model for "beating" between two cells that underlies several more sophisticated models of this type of behavior; shown how plateau potentials can arise from quiescent cells connected with reciprocal inhibition; sketched the outlines for ranges of synaptic threshold and strength required for oscillations in cases of two quiescent cells or two cells with plateau potentials, with the ability to generate similar maps of the ranges needed for other combinations; and predicted that some oscillations caused by reciprocal inhibition could be stopped by a suitably shaped current injection. We have done this without involving the reader in any sophisticated mathematics other than the geometric properties of two dimensional phase portraits. This was done with an extremely simple cell model that, nevertheless, captures the essential mechanism of many dynamical phenomena in small neural networks. If there is a well-defined relationship between it and a larger conductance-based model, the parameters and dynamics of the simple model map to parameters and dynamics of the larger model and thus provide a guide to the role of physiological parameters in the behavior of the larger model. Thus the simple model is a valuable tool for preliminary exploration of the dynamics of small networks.

Appendix: Relation of Our Model to a Conductance-Based Model

Consider the Morris-LeCar cell model, which has a leak conductance g_L with reversal potential V_L, a persistent calcium conductance g_{Ca} with activation variable $M_\infty(V)$, and slow potassium conductance g_K with time-dependent activation variable N. The calcium current is assumed to be so fast that it activates instantaneously. The time course for activation of the potassium activation variable N is given by the second equation below.

$$\begin{aligned} C\frac{\mathrm{d}V}{\mathrm{d}t} &= -g_L(V-V_L) \\ &\quad -g_{\mathrm{Ca}}M_\infty(V)(V-V_{\mathrm{Ca}}) \\ &\quad -g_K N(V-V_K) - I_{\mathrm{inj}} \\ \frac{\mathrm{d}N}{\mathrm{d}T} &= \lambda_N(V)(N_\infty(V)-N), \end{aligned}$$

where

$$\begin{aligned} M_\infty(V) &= \frac{1}{2}\left(1+\tanh\left(\frac{V-V_1}{V_2}\right)\right) \\ N_\infty(V) &= \frac{1}{2}\left(1+\tanh\left(\frac{V-V_3}{V_4}\right)\right) \\ \lambda_N(V) &= \phi_N \cosh\left(\frac{V-V_3}{2V_4}\right). \end{aligned}$$

Divide by g_L and set

$$\begin{aligned} \tau_m &= \frac{C}{g_L} \\ \mathrm{fast}(V, g_{\mathrm{Ca}}) &= (V-V_L) + \frac{g_{\mathrm{Ca}}}{g_L}M_\infty(V)(V-V_{\mathrm{Ca}}) \\ i_{\mathrm{inj}} &= \frac{I_{\mathrm{inj}}}{g_L} \\ \tau_N(V) &= \frac{1}{\lambda_N(V)} \\ q &= \frac{g_K}{g_L}N(V-V_K) \\ q_\infty(V) &= \frac{g_K}{g_L}N_\infty(V)(V-V_K). \end{aligned}$$

This gives

$$\begin{aligned} \tau_m\frac{\mathrm{d}V}{\mathrm{d}t} &= -(\mathrm{fast}(V, g_{\mathrm{Ca}}) + q + i_{\mathrm{inj}}) \\ \frac{1}{\lambda_N(V)}\frac{\mathrm{d}q}{\mathrm{d}t} &= \frac{1}{\lambda_N(V)}\frac{g_K}{g_L}\left[\frac{\mathrm{d}N}{\mathrm{d}t}(V-V_K) + N\frac{\mathrm{d}V}{\mathrm{d}t}\right] \\ &= \frac{g_K}{g_L}\Bigg[(N_\infty - N)(V-V_K) \\ &\qquad + \frac{1}{\lambda_N(V)}N\frac{\mathrm{d}V}{\mathrm{d}t}\Bigg] \\ &= q_\infty(V) - q + \epsilon, \end{aligned}$$

where, since $0 \le N \le 1$,

$$\begin{aligned} \epsilon &= \frac{1}{\lambda_N(V)}\frac{g_K}{g_L}N\frac{(\mathrm{fast}(V, g_{\mathrm{Ca}}) + q)}{\tau_m} \\ &\le \phi_N\frac{g_K}{C}(\mathrm{fast}(V) + q). \end{aligned}$$

For the majority of the time in one cycle, the phase point is on or near the fast nullcline $\frac{\mathrm{d}V}{\mathrm{d}t} = -(\mathrm{fast}(V) + q) = 0$, hence $\epsilon \approx 0$. For the remainder of a cycle, $\epsilon \not\approx 0$ only during the brief jumps from one arm of the fast nullcline to the other. Due to the difference in time constants, q changes by a negligible amount during a

jump, so the overall effect of ϵ is negligible. Dropping ϵ, we have reformulated the Morris-Lecar model as

$$\tau_m \frac{dV}{dt} = -(\text{fast}(V, g_{\text{Ca}}) + q + i_{\text{inj}})$$
$$\tau_N(V) \frac{dq}{dt} = q_\infty(V) - q.$$

If we now replace $\tau_N(V)$ by a constant $\tau_s = \tau_N(V_3) = 1/\phi_N$, then we have a model identical in form to the cell model given by Eqs. (1) and (2). The approximate map between the parameters of our model and the Morris-LeCar model is given by:

$$\sigma_s \approx \frac{g_K}{g_L}$$
$$\sigma_f \approx \frac{g_{\text{Ca}}}{g_L}$$
$$E_s \approx V_K$$
$$\tau_m = C/g_l$$
$$\tau_s \approx \tau_N(V_3).$$

Acknowledgments

A conversation with John Rinzel influenced this paper. We thank I-Teh Hsieh for assistance with the computer system. This work was supported by Office of Naval Research grant N00014-91-J-1720, National Institutes of Mental Health grant NH46899, and National Science Foundation grant IBN-9122712.

References

Abbot LF, Marder E, Hooper SL (1991) Oscillating networks: Control of burst duration by electrically coupled neurons. *Neural Computation* 3(4):487–497.

Anderson WW, Barker DL (1981) Synaptic mechanisms that generate network oscillations in the absence of discrete postsynaptic potentials. *J Exp. Zool.* 216(1):187–191.

Angstadt JD, Calabrese RL (1989). A hyperpolarization-activated inward current in heart interneurons of the medicinal leech. *J Neurophysiol*. 9:2846–2857.

Arbas EA, Calabrese RL (1987) Slow oscillations of membrane potential in interneurons that control heart-beat in the medicinal leech. *J. Neurosci* 7:3953–3960.

Arshavsky YI, Grillner S, Orlovsky GN, Panchin YV (1991) Central generators and the spatio-temporal pattern of movements. In Fagard J, Wolff PH, eds. The Development of Timing Control and Temporal Organization in Coordinated Action. Elsevier Science, Amsterdam. pp 93–115.

Arshavsky YI, Orlovsky GN, Panchin YV, Roberts A, Soffe SR (1993) Neuronal control of swimming locomotion: analysis of pteropod mollusc *Clione* and embryos of the amphibian *Xenopus*. *TINS* 16:227–233.

Bal T, Nagy F, Moulins M (1988) The pyloric central pattern generator in Crustacea: A set of conditional neuronal oscillators. *J. Comp. Physiol. A* 163:715–772.

Brown TG (1914) On the nature of the fundamental activity of the nervous centers together with an analysis of the conditioning of rhythmic activity in progression and a theory of the evolution of function in the nervous system. *J. Physiol*. 48:18–46.

Buchholtz F, Golowasch J, Epstein IR, Marder E (1992) Mathematical model of an identified stomatogastric ganglion neuron. *J. Neurophysiol*. 67(2):332–340.

Calabrese RL, Nadim F, Olsen OH (1995) Heartbeat control in the medicinal leech: A model system for understanding the origin, coordination, and modulation of rhythmic motor patterns. *J Neurobiol*. 27(3):390–402.

Cardi P, Nagy F (1994) A rhythmic modulatory gating system in the stomatogastric nervous system of *Homarus gammarus*. III. Rhythmic control of the pyloric CPG. *J. Neurophysiol*. 71(6):2503–2516.

Eisen JS, Marder E (1984). A mechanism for production of phase shifts in a pattern generator. *J. Neurophysiol*. 51(6):1375–1393.

Elson RC, Selverston AI (1992) Mechanisms of gastric rhythm generation in the isolated stomatogastric ganglion of spiny lobsters: Bursting pacemaker potentials, synaptic interactions and muscarinic modulation. *J. Neurophysiol*. 68(3):890–907.

Fitzhugh R (1961) Impulses and physiological states in theoretical models of nerve membrane. *Biophys J*. 1:445–466.

Friesen WO, Stent GS (1978) Neural circuits for generating rhythmic movements. *Ann. Rev. Biophys. Bioeng*. 7:37–61.

Getting PA (1989) Emerging principles governing the operation of neural networks. *Ann. Rev. Neurosci*. 12:185–204.

Golomb D, Guckenheimer J, Gueron S, (1993) Reduction of a channel-based model for a stomatogastric ganglion LP neuron. *Biol. Cybern*. 69(2):129–137.

Golowasch J, Marder E (1992). Ionic currents of the lateral pyloric neuron of the stomatogastric ganglion of ohe crab. *J Neurophysiol*. 67:318–331.

Golowasch J, Marder E (1992) Ionic currents of the lateral pyloric neuron of the stomatogastric ganglion of the crab. *J. Neurophysiol*. 67:318–331.

Gramoll S, Schimdt J, Calabrese RL(1994) Switching in the activity state of an interneuron that controls coordination of the hearts in the medicinal leech (*Hirudo medicinalis*). *J. Exp. Biol.* 186:157–171.

Graubard K (1978) Synaptic transmission without action potentials. *J. Neurophysiol* 41:1014–1025.

Graubard K, Raper JA, Hartline DK (1983) Graded synaptic transmission between identified spiking neurons. *J. Neurophysiol* 50:508–521.

Guckenheimber J, Labouriau IS (1993) Bifurcation of the Hodgkin-Huxley equations: A new twist. *Bull Math. Biol*. 55(5):937–952.

Hansel D, Mato G, Meunier C (1995) Synchrony in excitatory neural networks. *Neural Comp*. 5:307–337.

Harris-Warrick RM, Marder E (1991) Modulation of neural networks for behavior. *Ann. Rev. Neurosci.* 14:39–57.

Harris-Warrick RM, Flamm RE, Johnson BR, Katz PS, Kiehn O, Zhang B (1992a). Neuromodulation of small neural networks in Crustacea. In: Duce IR, ed. *Proceedings of Neurotox '91*, Elsevier Science, Amsterdam. pp. 305–321.

Harris-Warrick RM, Marder E, Selverston AI, Moulins M (1992b) Dynamic Biological Networks: the Stomatogastric Nervous System. MIT Press, Cambridge. Mass.

Harris-Warrick RM, Coniglio LM, Levini RM, Gueron S, Guckenheimer J (1995a). Dopamine modulation of two subthreshold currents produces shifts in activity of an identified motoneuron. *J Neurophysiol*. 74(4).

Harris-Warrick RM, Coniglio LM, Barazangi N, Guckenheimer J, Gueron S (1995b) Dopamine modulation of transient potassium current evokes phase shifts in a central pattern generator network. *J. Neurosci.* 15(1):342–358.

Hille B (1984) Ionic Channels of Excitable Membranes. Sinauer, Mass.

Hindmarsh JL, Rose RM (1984) A model of neuronal bursting using three coupled first order differential equations. *Proc. R. Soc. Lond. B* 221(1222):87–102.

Hindmarsh JL, Rose RM (1994a) A model for rebound bursting in mammalian neurons. (1994b). Resonance in a model of a mammalian neuron. (1994c). A model of intrinsic and driven spindling in thalamocortical neurons. *Phil. Trans. R. Soc. Lond. B* 346:129–150, 151–163, 165–183.

Johnson BR, Peck JH, Harris-Warrick RM (1991) Temperature sensitivity of graded synaptic transmission in the lobster stomatogastric ganglion. *J. Exp. Biol.* 156:267–285.

Kepler TB, Abbott LF, Marder E (1992) Reduction of conductance-based neuron models. *Biol. Cybern*. 66(5):381–387.

Kiehn O (1991) Plateau potentials and active integration in the "final common pathway" for motor behavior. *TINS* 14:68–73.

Kiehn O, Harris-Warrick RM (1992) Serotonin modulation of hyperpolarization-activated inward current and calcium-dependent outward current in a crustacean motor neuron. *J. Neurophysiol*. 68:496–508.

Kopell N, LeMasson G (1994) Rhythmogenesis, amplitude modulation, and multiplexing in a cortical architecture. *Proc. Natl. Acad. Sci. USA* 91:10586–10590.

Kopell N, Somers D (1995) Anti-phase solutions in relaxation oscillators coupled through excitatory interactions. *J. Math. Biol.* 33:261–280.

Kristan WB Jr (1980) Generation of rhythmic motor patterns. In: Pinsker HM, Willis WD, Jr. eds. *Information Processing in the Nervous System.* Raven Press, New York. pp. 241–261.

Llinas RR (1988) The intrinsic electrophysiological properties of mammalian neurons: Insights into central nervous system function *Science*. 242:1654–1664.

LoFaro T, Kopell N, Marder E, Hooper SL (1994) Subharmonic coordination in networks of neurons with slow conductances. *Neural Computation* 6(1):69–84.

Marder E (1991) Plateaus in time. *Current Biology* 1:326–327.

Marder E (1991). Modulation of neural networks for behavior. *Ann Rev Neurosci* 14:39–57.

McCormick DA, Pape HC (1990) Properties of a hyperpolarization-activated cation current and its role in rhythmic oscillation in thalamic relay neurones. *J. Physiol*. 431:291–318.

Miller J, Selverston AI (1982) Mechanisms underlying pattern generation in lobster stomatogastric ganglion as determined by selective inactivation of identified neurons. IV. Network properties of pyloric system. *J. Neurophysiol*. 48(6):1416–143.

Morris C, Lecar H (1981) Voltage oscillations in the barnacle giant muscle fiber. *Biophys. J.* 35:193–213.

Nadim F, Olsen OH, Schutter E, Calabrese RL (1995) Modeling the loeech heartbeat elemental oscillator I. Interactions of intrinsic and synaptic currents. *J. Comput. Neurosci.* 2:215–235.

Nagumo J, Arimoto S, Yoshizawa S (1962) An active pulse transmission line simulating nerve axon. *Proc. IRE* 50:2061–2070.

Opdyke CA, Calabrese RL (1994) A persistent sodium current contributes to oscillatory activity in heart interneurons in the leech. *J. Comp. Physiol. A* 175:781–789.

Perkel DH, Mulloney B (1974) Motor pattern production in reciprocally inhibitory neurons exhibiting postinhibitory rebound. *Science* 185:181–183.

Plant RE, Kim M (1976) Mathematical description of a bursting pacemaker neuron by modification of the Hodgkin-Huxley equations. *Biophys. J.* 16:227–244.

Raper J (1979a) Non-impulse-mediated synaptic transmission during the generation of a cyclic motor program. *Science* 205:304–306.

Raper J (1979b) Nonimpulse-mediated synaptic Transmission in the Stomatogastric Ganglion of the Spiny Lobster. Ph.D. thesis, University of California, San Diego.

Rose RM, Hindmarsh JL (1985) A model of a thalamic neuron. *Proc. R. Soc. Lond B* 225(1239):161–193.

Rose RM, Hindmarsh JL (1989a) The assembly of ionic currents in a thalamic neuron. I. The three-dimensional model (1989b). The assembly of ironic currents in a thalamic neuron. II The stability and state diagrams. (1989c) The assembly of ironic currents in a thalamic neuron. III The seven-dimensional model. *Proc. R. Soc. Lond. B* 237:267–288, 289–312, 313–334.

Rowat PF, Selverston AI (1993) Modeling the gastric mill central pattern generator with a relaxation-oscillator network. *J. Neurophysiol.* 70(3):1030–1053.

Russell DF (1985) Neural basis of teeth coordination during gastric mill rhythms in spiny lobsters. *J. Exp. Biol.* 114:99–119.

Satterlie RA (1985) Reciprocal inhibition and postinhibitory rebound produce reverberation in a locomotor pattern generator. *Science* 229:402–404.

Selverston AI (1993) Neuromodulatory control of rhythmic of behaviors in invertebrates. *Int. Rev. Cytology.* 147:1–24.

Skinner FK, Kopell N, Marder M (1994) Mechanisms for oscillation and frequency control in reciprocal inhibitory model neural networks. *J. Comput. Neuroscience* 1(1/2):69–88.

Somers D, Kopell N (1993) Rapid synchronization through fast threshold modulation. *Biol. Cybern*. 68:393–407.

Terman D, Wang DeL (1995) Global competition and local cooperation in a network of neural oscillators. *Physica D* 81:148–176.

Van Vreeswijk C, Abbott LF, Ermentrout GB (1994) When inhibition and not excitation synchronizes neural firing. *J. Comput. Neurosci*. 1:313–321.

Wang DeL, Terman D (1994) Locally excitatory globally inhibitory oscillator networks. *IEEE Trans. on Neural Networks* 6(1):283–286.

Wang X-J (1994) Multiple dynamical modes of thalamic relay neurons: rhythmic bursting and intermittent phase-locking. *Neuroscience* 59(1):21–31.

Wang X-J, Rinzel J (1992) Alternating and synchronous rhythms reciprocally inhibitory model neurons. *Neural Computation* 4:84–97.

Wang X-J, Rinzel J (1993) Spindle rhythmicity in the reticularis thalami nucleus: Synchronization among mutually inhibitory neurons. *Neuroscience* 53(4):899–904.

Wang X-J, Golomb D, Rinzel J (1995) Emergent spindle oscillations and intermittent burst firing in a thalamic model: Specific neuronal mechanisms. *Proc. Natl. Acad. Sci. USA* 92:5577–5581.

Wiens TJ (1982) Small systems of neurons: Control of rythmic and reflex activities. In: Sandeman DC, Atwood HL, eds. Neural Integration and Behavior. Academic Press, New York.